Coordination Chemistry Reviews 255 (2011) 837–860

Contents lists available at ScienceDirect

Coordination Chemistry Reviews

journal homepage: www.elsevier.com/locate/ccr

Review

Dithiolene radicals: Sulfur K-edge X-ray absorption spectroscopy and Harry's intuition

Stephen Sproules*, Karl Wieghardt

Max-Planck-Institut für Bioanorganische Chemie, Stiftstrasse 34-36, D-45470 Mülheim an der Ruhr, Germany

Contents

ARTICLE INFO

Article history:
Received 14 September 2010
Accepted 3 December 2010
Available online 16 December 2010

Keywords:
Dithiolene
Transition metal
Ligand radical
Spectroscopy
Redox noninnocence
Electronic structure
Geometry

ABSTRACT

The 50-year old debate regarding the true electronic structure of transition metal bis(dithiolene) complexes has been revolutionized recently by involvement of sulfur K-edge X-ray absorption spectroscopy (XAS) to directly probe the sulfur composition of the frontier orbitals. In concert with other spectroscopic methods, and increasingly theoretical calculations, a more accurate electronic structure description has been delivered. The methodology developed has also been applied to mono(dithiolene) and tris(dithiolene) coordination complexes whereby the electronic structure of these systems has been defined in terms of physical oxidation levels of both metal and ligand, ultimately providing direct experimental evidence for the noninnocence of dithiolene ligands.

Abbreviations: XAS, X-ray absorption spectroscopy; S, total spin state; S_L, spin state of ligand(s); S_M, spin state of metal; g, g-value; A, magnetic hyperfine interaction; δ, isomer shift; ΔE_Q, quadrupole splitting; I, nuclear spin; $I(S)$, transition dipole integral; DFT, density functional theory; BS, broken symmetry; MO, molecular orbital; ZORA, zeroth-order regular approximation; SOMO, singly occupied molecular orbital; HOMO, highest occupied molecular orbital; LUMO, lowest unoccupied molecular orbital; JACS, Journal of the American Chemical Society; CT, charge transfer; LLCT, ligand-to-ligand charge transfer; IVCT, intervalence charge transfer; IR, infrared; UV, ultraviolet; Vis, visible; EPR, electron paramagnetic resonance; ENDOR, electron nuclear double resonance; ESEEM, electron spin echo envelope modulation; Z_{eff}, effective nuclear charge; cyclam, 1,4,8,11-tetraazacyclotetradecane; tren, tris(2-aminoethyl)amine; dtc, diethyldithiocarbamate; bpy, bipyridine; Θ, trigonal twist angle; α, chelate fold angle.

* Corresponding author.
E-mail address: sproules@mpi-muelheim.mpg.de (S. Sproules).

0010-8545/$ – see front matter © 2010 Elsevier B.V. All rights reserved.
doi:10.1016/j.ccr.2010.12.006

1. Introduction

When in 1965 Harry Barkus Gray penned a paper entitled "The Myth of Nickel(III) and Nickel(IV) in Planar Complexes" [1], he reaffirmed that $[Ni(dithiolene)_2]^{0/1-}$ exhibited chemical and physical properties incompatible with their Ni(IV) and Ni(III) formal oxidation states [2], respectively, and then proceeded to ignite a vigorous debate by announcing that these complexes are best viewed as *metal stabilized radical-ligand systems*. At this stage, transition metal dithiolene chemistry was in its formative years having burst on the scene in the early 1960s owing to the targeted synthesis of dithiolate ligands, either *cis*-ethylene-1,2-dithiolates or aromatic-1,2-dithiolates, and their subsequent reaction with metal salts, principally chlorides. They generated considerable interest given their prolific display of intense colors, multiple reversible redox processes, irregular geometries, and, most notably, nonclassical electronic structures. It was the last that precipitated the great dithiolene war of the 1960s; an intense volley of words bundled into JACS communications interspersed by the occasional full paper that were hurled between the key protagonists of the era who fought over the ground state description of bis(dithiolene)nickel. The outcome of which not only made the careers of many of today's notable inorganic chemists, but also gave the field its first redox noninnocent bidentate ligand, the dithiolene (Scheme 1).

In their original synthetic paper of 1963 [3], Gray and co-workers isolated the monoanionic bis(dithiolato)nickel complex, that of $[Ni(tdt)_2]^{1-}$ ($S = 1/2$) where $(tdt)^{2-}$ is toluene-3,4-dithiolate, and defined this as Ni(I) bound by two dithiolate radical anions. The unpaired electron on each radical ligand was said to be paired with its partner in one of the π molecular orbitals (MOs) of these square planar complexes. This implied that the Ni(I) d^9 central ion bore the unpaired spin, though, as pointed out by the Harvard team of Maki, Edelstein, Davison, and Holm [4], as well as Schrauzer and his colleagues in Munich [5], this would not generate the observed rhombic EPR signal. The preceding paper detailed the preparation of $[M^{II}(mnt)_2]^{2-}$ complexes, where $(mnt)^{2-}$ is maleonitriledithiolate, with divalent metals Co, Ni, Pd, Pt, Cu, and Zn [6]. The ground state for $[Ni^{II}(mnt)_2]^{2-}$ ($S = 0$) calculated using a modified Wolfsberg–Helmholz method was described as $(4b_{2g})^2(4a_g)^2 = {}^1A_g$ [7], where $4a_g$ is the $d_{x^2-y^2}$ orbital and $4b_{2g}$ the d_{xz} orbital; the crystal structure soon followed [8]. Gray et al. regrouped by stating that these frontier orbitals were "definitely more ligand than metal" in character, and defined the ground state configuration for $[Ni^{II}(mnt)(mnt^{\bullet})]^{1-}$ ($S = 1/2$) as.$(4b_{2g})^2(4a_g)^1 = {}^2A_g$ containing one mnt radical anion [7]; the nickel ions in both species bear a +II physical oxidation state [2].

The first neutral complex, $[Ni(pdt)_2]^0$ ($S = 0$), where $(pdt)^{2-}$ is 1,2-diphenyl-1,2-ethylenedithiolate, was prepared by Schrauzer and Mayweg from the esoteric reaction of nickel sulfide and diphenylacetylene [9]. They deduced a square planar structure with a Ni(II) d^8 central ion where the +II charge was compensated by "two electrons occupying low-lying π-MO extending over the whole complex." Two degenerate ligand-based unoccupied orbitals, identified as $2b_{2g}$ and $2b_{1u}$ MOs [5], are key to the electronic structure of the neutral complex. Since the former can only interact with the metal $d_{xz,yz}$ orbitals, it is destabilized with respect to the $2b_{1u}$ MO, to give an ordering of $nd < 2b_{1u} < 2b_{2g} < (n+1)p$. The neutral complex was best described by valence bond resonance forms with a combination of dithiolate and dithioketone forms of the ligand (Scheme 1), where the true electronic structure lies somewhere between these extremes (Scheme 2). There were certainly structural data to give credence to such a formulation, with a shortening of the C–S and lengthening of the C–C bonds as charge was added to the basic $[MS_4]$ unit. As a consequence, the associated infrared (IR) stretching frequencies increased and decreased, respectively [10]. From this platform, Schrauzer et al. defined the intense low-energy charge transfer (CT) band in the electronic spectra of $[Ni(pdt)_2]^0$ ($S = 0$) and $[Ni(pdt)_2]^{1-}$ ($S = 1/2$) as an inner-π-transition $2b_{1u} \rightarrow 2b_{2g}$ [5,10]. The dianion exhibited a completely different absorption profile consistent with a filled $2b_{2g}$ MO; the three-membered electron transfer series is related by occupation of this level. Therefore, as stated by Schrauzer, "...the reduction of the complexes does not change the formal +II oxidation state of the nickel, palladium, or platinum atoms" [10].

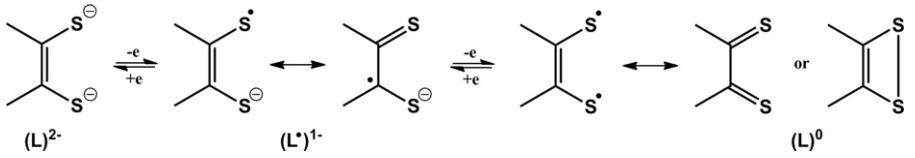

Scheme 1. The three oxidation levels of a dithiolene ligand.

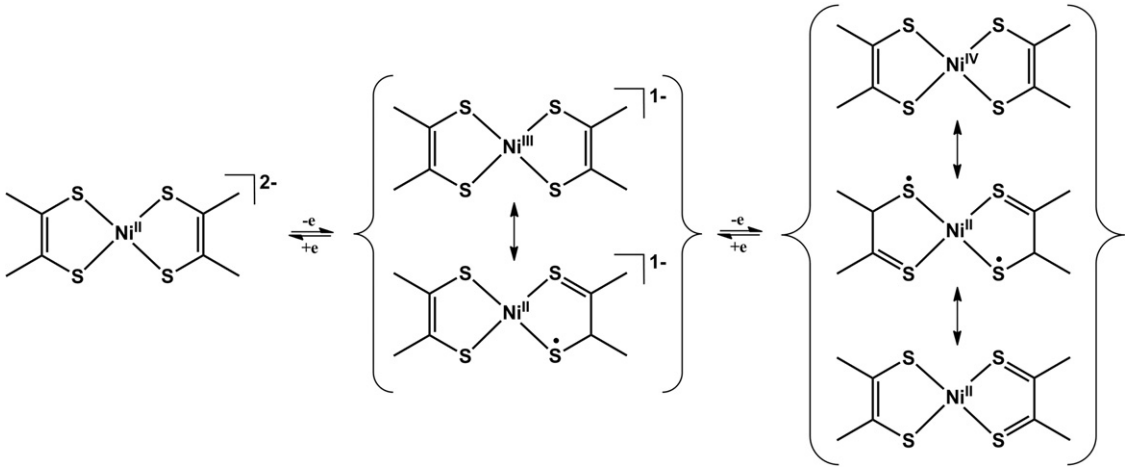

Scheme 2. Limiting ligand and metal oxidation levels for planar members of the electron transfer series $[Ni(L)_2]^z$ ($z = 0, 1-, 2-$) [16].

The Harvard team joined Schrauzer and Mayweg in declaring a $^2B_{2g}$ ground state ($^2B_{3g}$ in the original report; the *y*-axis defined as bisecting the dithiolene ligands) for the monoanionic bis(dithiolene)nickel complex [4], however there was a difference of opinion as to its composition. Their work was initiated by the possibility of isolating the three members of an electron transfer series differing only in the total number of valence electrons [11]. In doing so, they described the first ever four-coordinate paramagnetic complexes of Pd and Pt [12]. A rigorous electron paramagnetic resonance (EPR) spectroscopic study of $[Ni(mnt)_2]^{1-}$ ($S = 1/2$) afforded theoretical expressions for the *g* and *A* tensors using perturbation theory. The singly occupied molecular orbital (SOMO) for these planar systems (b_{2g}) was described as 50% metal in character and the ground state declared a d^3-hole $(d_{xz})^1(d_{xy})^2$ configuration implying a low-spin Ni(III) d^7 central ion [4]. Schrauzer and Mayweg settled on 18% Ni character maintaining a Ni(II) d^8 ion [5], before promptly revising that to 51% a few years later with extended Wolfsberg–Helmholz calculations [13] bringing it into excellent agreement with a single-crystal EPR study on $NBu_4[Ni(mnt)_2]$ [14]. In a subsequent study aimed at defining the metal contribution to the SOMO through deviation of the *g*-tensor [15], the Harvard team concluded that, although the spectrum did not favor – in their parlance – a cationic-stabilized free-radical in $[Ni–S_4]^{1-}$ compounds, overall the method was inadequate at defining the point at which "the description is changed from ligand free radical to metal-localized radical;" this is currently a subjective matter.

It was not until the rise of density functional theory (DFT) that a re-examination of the bis(dithiolene)nickel series was undertaken. Early Hückel and Wolfsberg-Helmholz MO calculations were clearly too primitive and too varying in their description of the frontier orbitals to give an unambiguous result. We had to wait 30 years before a seminal study by one of the grand sages of dithiolene chemistry was published in 1998, along with crystallographic characterization of the three-membered electron transfer series $[Ni(mdt)_2]^z$ ($z = 0, 1-, 2-$), where $(mdt)^{2-}$ is 1,2-dimethyl-1,2-ethylenedithiolate [16]. Geometry optimizations accurately reproduced the X-ray structures of all members, including the experimental trends in the Ni–S, C–S and C–C bond distances when passing from the dianionic to monoanionic and neutral complexes. Furthermore, it was shown that S 3p character accounted for ~60% of the electroactive $5b_{2g}$ MO in the neutral and monoanionic species; reduced to 50% in the dianionic compound [16], with the Ni $3d_{xz}$ content calculated to be 13.3%, 19.5%, and 38.9% for the neutral, monoanion, and dianion complexes, respectively; a Ni(II) d^8 central ion in each. More recently, an elaborate correlated *ab initio* study on the $[Ni(tbbdt)_2]^z$ ($z = 0, 1-, 2-$) series, where $(tbbdt)^{2-}$ is Sellmann's 3,5-di-*tert*-butylbenzene-1,2-dithiolate ligand [17]. Its goal was to address the singlet diradical nature of the neutral compound, and followed a similar study of analogous the bis(diimine)nickel complex [18]. A diradical character of 32% was computed, though it was emphatically emphasized that this value is heavily dependent on the theoretical method used, differing quite markedly from a previous foray using DFT calculations [19]. This diradical character was supported by the magnitude of the singlet–triplet gap that was correlated to the very intense ligand-to-ligand charge transfer (LLCT) band in the near-infrared (NIR) region of the electronic spectrum [17].

The success of these later theoretical studies to elucidate the electronic structure of the bis(dithiolene)nickel electron transfer series, and related series with other transition metals, was the correlation of experiment with theory by calculating physical observables. However, sulfur itself is amongst the most spectroscopically silent elements in the periodic table, with only the ^{33}S isotope ($I = 3/2$, 0.75% natural abundance) offering something of a glimmer, there is almost nothing physical to calculate. Enter sulfur K-edge X-ray absorption spectroscopy (XAS) to enliven electronic structure studies of dithiolene compounds. The technique is element specific and directly probes the nature of the sulfur atoms in a given system without interference from other absorbers. This account presents an overview of the way in which sulfur K-edge XAS has revolutionized the study of transition metal dithiolene chemistry; a list of the ligands and their abbreviations is presented in Scheme 3. For the first time, we have a method to directly measure the oxidation level of the dithiolene ligand and in conjunction with metal K- and L-edges, the physical oxidation state of the central metal ion as well.

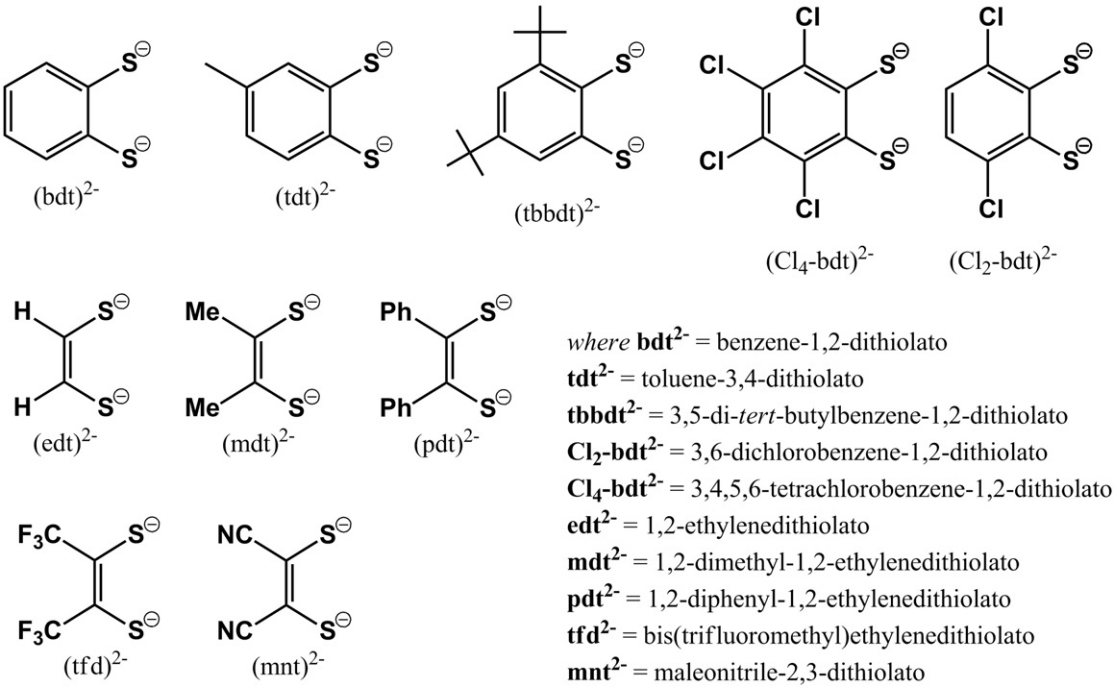

Scheme 3. Dithiolene ligands and their abbreviations.

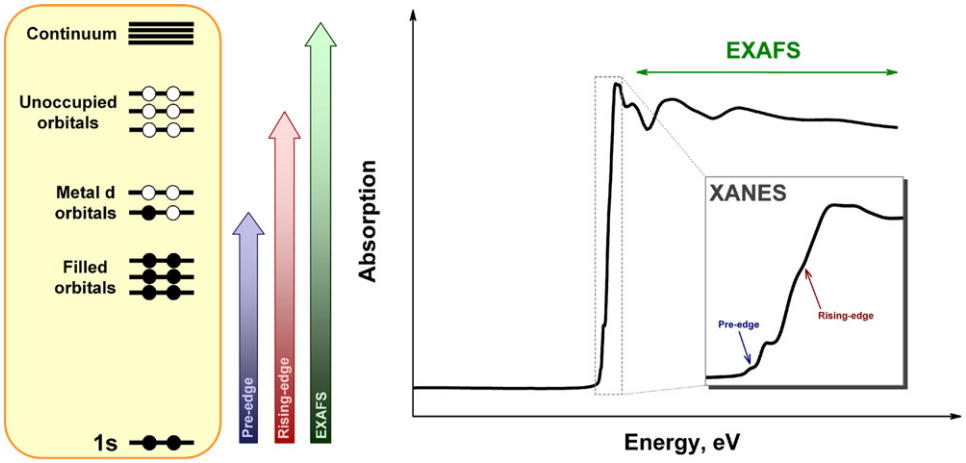

Fig. 1. Simplified depiction of the components of a metal K-edge XAS experiment: Excitation of a core 1s electron to vacant d orbitals generates the pre-edge features whereas the rising-edge is dominated by dipole-allowed 1s → *n*p transitions (XANES). Beyond the edge, the input energy from the X-ray beam is sufficient to eject the electron from the absorbing atom which emanates as a photoelectron that interacts with electrons of the surrounding atoms giving rise to oscillations in the spectrum (EXAFS).

2. The experiment

All sulfur K-edge data presented in this review were measured at the Stanford Synchrotron Radiation Lightsource (*née* Stanford Synchrotron Radiation Laboratory) under ring conditions of 3 GeV and 60–100 mA. The experiments were performed on the 54-pole wiggler beamline 6-2 or 4-3 in high field (10 kG) mode with a fully tuned Si(1 1 1) double crystal monochromator followed by a Ni-coated harmonic rejection mirror. Details of the optimization of this setup have been previously described [20]. Metal K-edge data were measured using a focused 20-pole wiggler beamline 7-3. A Si(2 2 0) monochromator was utilized for energy selection, and a harmonic rejection mirror was present to minimize higher harmonic components in the X-ray beam.

In an overly simplified picture (Fig. 1), K-edge X-ray absorption spectra arise from promotion of a core 1s electron to a vacant orbital on an absorbing atom. This part of the spectrum is named X-ray absorption near-edge structure (XANES) and provides electronic structure information about the material under examination. As more energy is applied – beyond the edge – the core electron is jettisoned from the absorbing atom and emanates outward as a photoelectron interacting with the immediate neighbors generating an oscillating pattern in the spectrum. This post edge region of the spectrum is coined extended X-ray absorption fine structure (EXAFS) since the oscillations arising from the interference of the photoelectron with electrons in the surrounding atoms yields geometric information about the system, mainly distances.

The XANES part of the experiment is subdivided into pre-edge and rising-edge regions. The rising-edge is dominated by electric dipole-allowed 1s → *n*p transitions (Fig. 1). The pre-edge region in metal K-edge spectra arises from electric dipole-forbidden but quadrupole-allowed 1s → *n*d that can gain intensity through mixing of metal p character via departure from centrosymmetry, for example a twist from square planar to tetrahedral. This also affects the ligand field and hence the transition energy. The K-edge is a direct measure of the effective nuclear charge (Z_{eff}) of an element, i.e. its oxidation state, with the core 1s orbital shifting to deeper binding energy with increasing Z_{eff}. This gives rise to the generally accepted rule of thumb that a 1 eV shift in the edge to higher energy corresponds to an increase in the oxidation state by one unit.

The perfect compliment to a metal K-edge is the sulfur K-edge. It follows the same principles described above except that its pre-edge features result from electric dipole-allowed S 1s → 3p transition (Fig. 2). There are two ways to create a vacant site in the S 3p orbitals, namely removing an electron generating a sulfur-centered radical and a partial hole from covalent M–S bonding that shifts electron density from filled S 3p orbitals to vacant metal d orbitals. Thus, S K-edge probes all singly occupied and unoccupied orbitals of a transition metal complex that have S 3p character, and therefore is a direct measure of the covalency of a metal–sulfur bond whereby the peak intensity reflects the amount of S 3p content of the absorbing orbital [21,22]. The oxidation level of the sulfur atoms will be reflected in the pre- and rising-edge energies, but usually with more than one sulfur atom present, as is the case for a dithiolene ligand, a 1 eV shift is rarely observed. Furthermore, changes in complex geometry can counteract this shift since the ligand field is affected.

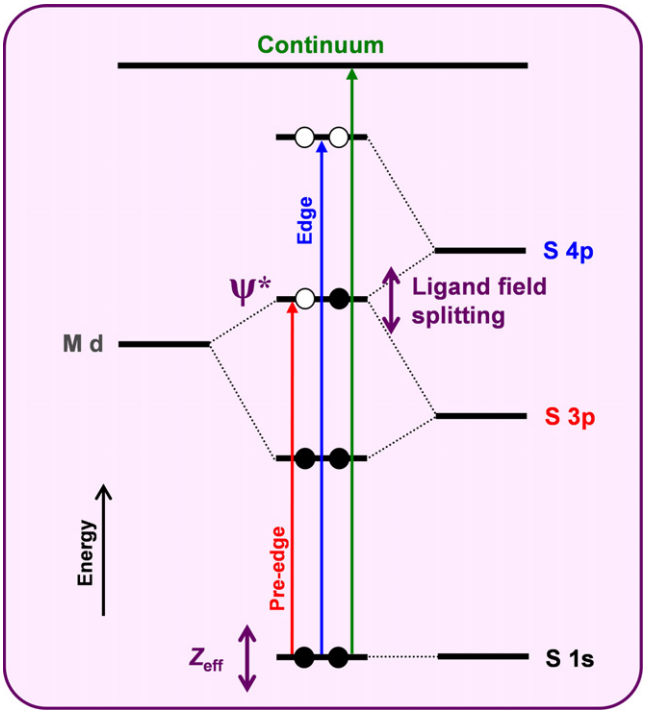

Fig. 2. Simplified molecular orbital manifold indicating the pre-edge and edge transitions in a sulfur K-edge XAS spectrum.

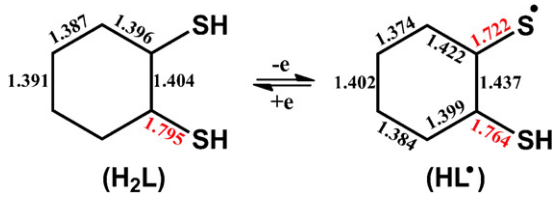

Fig. 3. Bond distances (Å) from a geometry optimized benzene-1,2-dithiol (H_2L) and its one-electron oxidized form, HL [23].

This review is directed at presenting an overview of the impact that sulfur K-edge XAS studies have provided in describing the electronic structure of transition metal dithiolene complexes. The existence of a monoanionic dithiolene radical ligand $(L^{\bullet})^{1-}$, is fingerprinted by a low-energy (typically <2470 eV) pre-edge peak defined as a S 1s → L• transition. In many cases, particularly when S K-edge spectra of two or more members of an electron transfer series have been recorded, a simple qualitative examination is sufficient to determine metal and ligand oxidation levels. As will be evident throughout, S K-edge XAS works in concert with metal K-edge XAS, and many other spectroscopic and increasingly, theoretical methods, to give an electronic structure description for transition metal complexes with one, two, or three dithiolene ligands.

3. Mono(dithiolene) complexes

Proper determination of the electronic structure of transition metal dithiolene complexes requires identification of structural and spectroscopic features that allow the unequivocal detection and characterization of monoanionic dithiolene radicals. Many authors have attempted to discern between dithiolate(2−) and its monoanionic radical form in a given complex by their crystallographically determined structural parameters (Fig. 3).

The underlying assumption has always been that the phenyl ring of an aromatic-1,2-dithiolate has six equidistant C–C bonds or displays two short and four long C–C bonds in the radical form. Additionally, the C–S bonds would shrink upon oxidation of a dithiolate dianion (Fig. 3). This behavior is firmly ensconced in dioxolene systems (catecholates and semiquinonates) [24,25] but is missed in dithiolene chemistry owing to the overwhelming parentage by the sulfur atoms of the unpaired spin that curtails the quinoid-like distortion such that it is rarely outside the crystallographic 3σ level (Fig. 4) [17,23].

Sulfur K-edge X-ray absorption spectroscopy is the ideal experimental probe of radical character in transition metal dithiolene complexes. Specifically, the quantification of sulfur 3p content

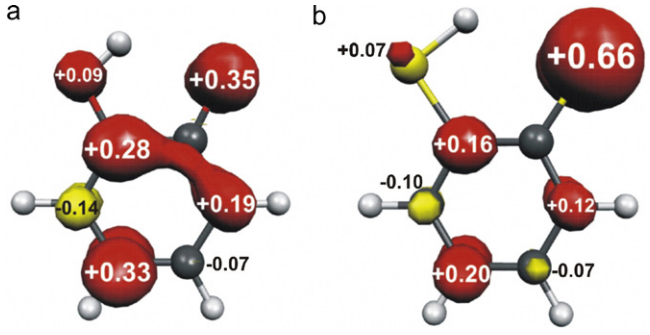

Fig. 4. Mulliken spin densities of the radicals (a) *o*-benzosemiquinone and (b) *o*-dithiobenzosemiquinone [23].

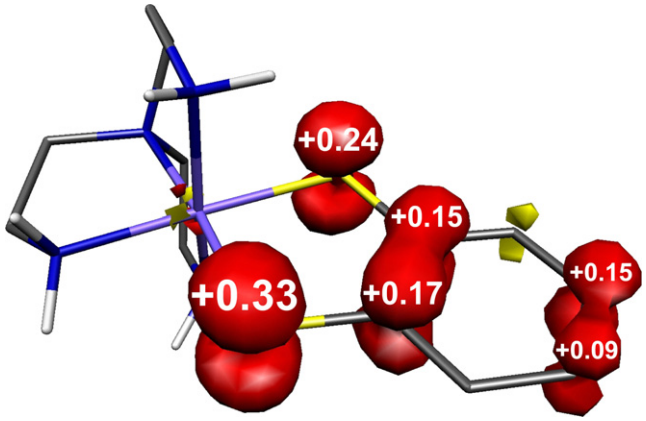

Fig. 5. Spin density plot for $[Co^{III}(tren)(bdt^{\bullet})]^{2+}$ obtained from a Mulliken spin population analysis [23].

in the unoccupied antibonding valence orbitals determines their covalency and highlights the noninnocence of dithiolene ligands in situations that give rise to an inverted bonding scenario.

3.1. Iron and cobalt

In a recent report it was shown that it is possible to electrochemically generate a one-electron oxidized form of a 1,2-dithiolate ligand while coordinated to cobalt [23]. The precursor $[Co^{III}(tren)(bdt)](PF_6)$ ($S = 0$) is an archetypal Werner-type complex with a central low-spin Co(III) d^6 ($S_{Co} = 0$), neutral tren (tren = tris(2-aminoethyl)amine) and diamagnetic $(bdt)^{2-}$ (bdt = benzene-1,2-dithiolate). The oxidized product $[Co^{III}(tren)(bdt^{\bullet})]^{2+}$ ($S = 1/2$) possessed an S,S′-coordinated dithiolene radical in an experiment directly analogous of an *O*,*O*′-coordinated *o*-benzosemiquinonate(1−) ligand $(sq^{\bullet})^{1-}$. The latter was characterized by X-ray crystallography [26], where short C–O and a quinoid distortion of the aromatic ring (four long and two short C–C bonds) supported such a formulation. Perhaps the most important evidence for a coordinated $(sq^{\bullet})^{1-}$ ligand came from its EPR spectrum, with a ^{59}Co ($I = 7/2$, 100% natural abundance) magnetic hyperfine interaction of $\langle A_{Co}\rangle = 9.76$ G [26]. For electrochemically generated $[Co^{III}(tren)(bdt^{\bullet})]^{2+}$, a value of $\langle A_{Co}\rangle = 14$ G was recorded [23], slightly larger due to more covalent Co–S bonds. A clear distinction is made when this EPR spectrum is compared with a genuine $Co^{IV}S_6$ ($S = 1/2$) center in $[Co^{IV}(dtc)_3]^{1+}$, where $(dtc)^{1-}$ is diethyldithiocarbamate, with $\langle A_{Co}\rangle = 140$ G [27]. So electron-starved is the Co(IV) d^5 central ion in $[Co^{IV}(dtc)_3]^{1+}$ that it eventually consumes itself generating $[Co^{III}{}_2(dtc)_5]^{2+}$ with the more satisfying d^6 configuration, such that it is almost impossible to entertain a $[Co^{IV}(tren)(bdt)]^{2+}$ electronic structure for this electrochemically oxidized dication. DFT calculations elegantly visualize the electronic structure as is shown by the Mulliken spin density plot presented in Fig. 5 with the unpaired electron found almost exclusively (only 3% Co) on the dithiolene ligand [23].

The analogous Fe compound, $[Fe^{III}(cyclam)(tdt)](PF_6)$ ($S = 1/2$) is again a Werner-type complex with an octahedral low-spin Fe(III) d^5 ($S_{Fe} = 1/2$) central ion bound by the tetradentate, closed-shell cyclam (cyclam = 1,4,8,11-tetraazacyclotetradecane) and bidentate $(tdt)^{2-}$ (tdt = toluene-3,4-dithiolate) ligands [28]. Its cyclic voltammogram displays one reversible reduction and one reversible oxidation wave to neutral and dicationic species, respectively. While it is trivial to diagnose the neutral species as $[Fe^{II}(cyclam)(tdt)]^0$ ($S = 2$) with a high-spin Fe(II) d^6 ion shown by Mössbauer spectroscopy, the identity of the oxidation as metal- or ligand-centered is not immediately apparent, since unlike cobalt, +IV and higher oxidation states feature prominently in

$$[Fe^{II}(cyclam)(tdt)]^{0} \underset{+e}{\overset{-e}{\rightleftharpoons}} [Fe^{III}(cyclam)(tdt)]^{1+}$$
$$(S = 2) \qquad (S = {}^{1}/_{2})$$
$$+e \uparrow\downarrow -e$$
$$[Fe^{III}(cyclam)(tdt^{\bullet})]^{2+}$$
$$(S = 0)$$

Scheme 4. The three-membered electron transfer series of $[Fe^{III}(cyclam)(tdt)]^{z}$ ($z = 0, 1+, 2+$) [28].

iron chemistry. The two possibilities $[Fe^{IV}(cyclam)(tdt)]^{2+}$ ($S = 1$) or $[Fe^{III}(cyclam)(tdt^{\bullet})]^{2+}$ ($S = 0$) were distinguished by Mössbauer spectroscopy – the bread and butter approach for iron. The precursor $[Fe^{III}(cyclam)(tdt)]^{1+}$ ($S = 1/2$) is characterized by an isomer shift $\delta = 0.38\ mm\ s^{-1}$ and quadrupole splitting $\Delta E_Q = 1.80\ mm\ s^{-1}$. The oxidized dication has $\delta = 0.29\ mm\ s^{-1}$ and $\Delta E_Q = -2.24\ mm\ s^{-1}$ which is quite similar to the starting material, however a $0.09\ mm\ s^{-1}$ lowering of the isomer shift does not entirely eliminate the Fe(IV) possibility. Applied-field Mössbauer measurements settled the argument, as the absence of an internal magnetic field around the iron nucleus rules out an Fe(IV) $S = 1$ species. DFT calculations confirmed this as a ligand-centered oxidation to give $[Fe^{III}(cyclam)(tdt^{\bullet})]^{2+}$ ($S = 0$) in particular by calculation of the Mössbauer parameters; the electron transfer series is defined in Scheme 4. The diamagnetic ground state arrives via strong antiferromagnetic coupling of the metal- and ligand-centered unpaired electrons that classifies this species as a singlet diradical; the Mulliken spin density plot is shown in Fig. 6 [28].

X-ray absorption spectroscopy truly cemented the message, with a combination of metal and ligand K-edge measurements. The Fe K-edge spectra of $[Fe^{III}(cyclam)(tdt)]^{1+}$ ($S = 1/2$) and $[Fe^{III}(cyclam)(tdt^{\bullet})]^{2+}$ ($S = 0$) exhibit similar rising-edge energies, and more importantly, similar pre-edge peaks at 7112.2 eV for $[Fe^{III}(cyclam)(tdt)]^{1+}$ and 7112.5 eV for $[Fe^{III}(cyclam)(tdt^{\bullet})]^{2+}$ indicating a similar effective nuclear charge (Z_{eff}) at Fe, corroborating the Mössbauer spectral parameters. Had the metal been oxidized, ~1 eV shift to higher energy would have been anticipated. The sulfur K-edge XAS spectra are shown in Fig. 7 and the existence of a dithiolene radical is abundantly clear from the low-energy pre-edge peak at 2469.6 eV in the spectrum of $[Fe^{III}(cyclam)(tdt^{\bullet})]^{2+}$: the dithiolene radical fingerprint. There are two other pre-edge peaks at 2471.1 and 2472.6 eV. The S K-edge

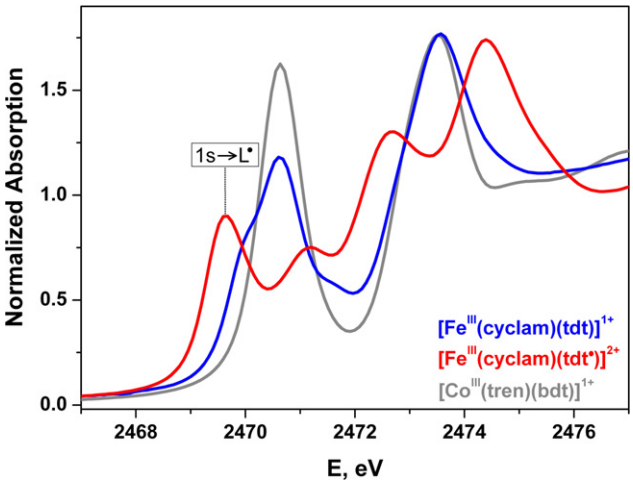

Fig. 7. Comparison of the normalized S K-edge spectra of $[Fe^{III}(cyclam)(tdt)]^{1+}$, $[Fe^{III}(cyclam)(tdt^{\bullet})]^{2+}$, and $[Co^{III}(tren)(bdt)]^{1+}$ [28].

spectrum of $[Fe^{III}(cyclam)(tdt)]^{1+}$ is noticeably devoid of any peak below 2470 eV – no dithiolene radical. However, this being Fe chemistry, it is never a simple as it seems, with a pre-edge shoulder at 2470.0 eV. This is defined as a transition to the t_{2g} singly occupied orbital (SOMO) which gains intensity from a weak covalent interaction between the Fe $3d_{xz}$ orbital and a π orbital of the dithiolate ligand, thus indicating a small contribution from the $[Fe^{II}\text{-}tdt^{\bullet}]^{1+}$ resonance structure. The two remaining peaks are defined as transitions to σ^* MOs (Fe e_g orbitals) which are split by multiplet effects, rarely reported for S K-edge spectra. The calibrant, the S K-edge spectrum of $[Co^{III}(tren)(bdt)]^{1+}$ ($S = 0$) shows only one pre-edge peak at 2470.6 eV consistent with its aforementioned electronic structure. The peak is due to $1s \rightarrow Co\text{–}S\ \sigma^*$ transitions.

This exhaustive spectroscopic study was elegantly supported by DFT calculations. Specifically, the qualitative validity of an open-shell singlet ground state description in the reproduction of the correct number of peaks by TD-DFT calculation of the S K-pre-edge spectrum. As demonstrated in Fig. 8, the simple closed-shell singlet ground state from a nonbroken symmetry, spin-restricted calculation fails to account for the experimental S K-pre-edge spectral profile. Only the BS(1,1) singlet diradical solution accommodates both the number and the intensity of the pre-edge region for $[Fe^{III}(cyclam)(tdt^{\bullet})]^{2+}$. Furthermore, the singlet diradical solution

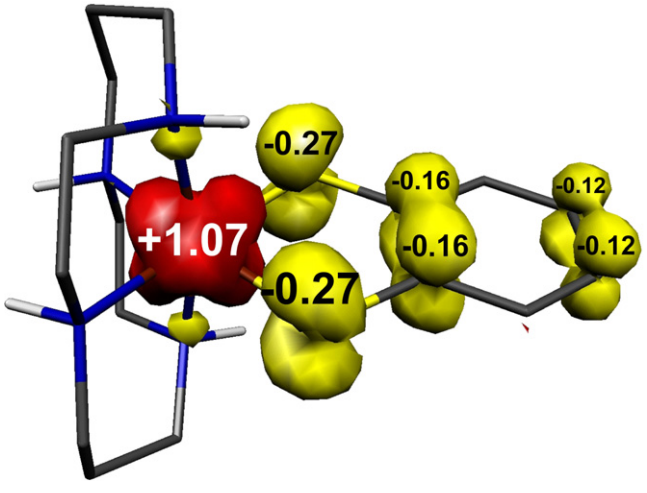

Fig. 6. Spin density plot for $[Fe^{III}(cyclam)(bdt^{\bullet})]^{2+}$ obtained from a Mulliken spin population analysis [28].

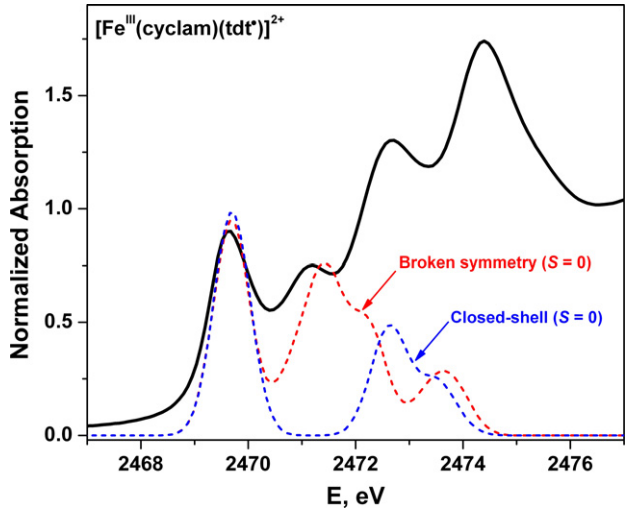

Fig. 8. Comparison of the calculated BS(1,1) open-shell singlet and spin-restricted closed-shell spectra with the experimental data [28].

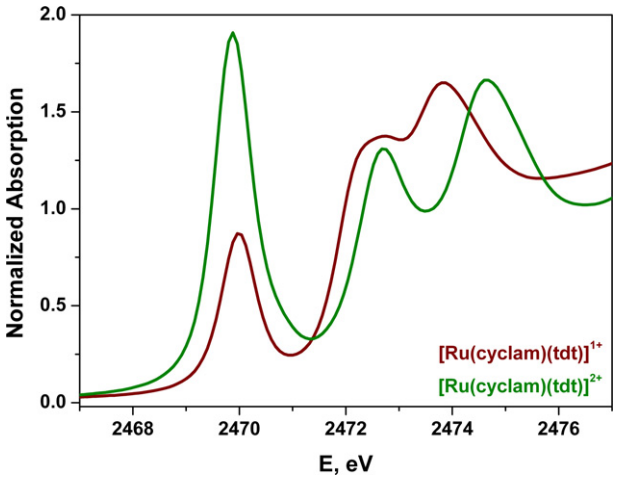

Fig. 9. Overlay of the normalized S K-edge spectra of $[Ru(cyclam)(tdt)]^{1+}$, and $[Ru^{III}(cyclam)(tdt)]^{2+}$ [30].

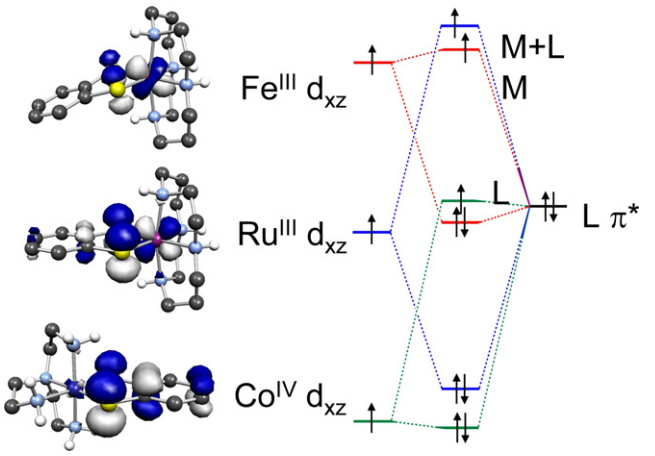

Fig. 10. Simplified bonding scheme for the π interactions in isoelectronic $[Fe^{III}(cyclam)(tdt)]^{1+}$, $[Ru(cyclam)(tdt)]^{1+}$, and $[Co^{III}(tren)(bdt^{\bullet})]^{2+}$ ($S = 1/2$) [30].

was a significant 7 kcal mol^{-1} more stable than the closed-shell, spin-restricted $S = 0$ approach.

3.2. Ruthenium

In contrast to this apparently straightforward description of the electronic structure for the Fe series, it has been subsequently shown that ruthenium is a world apart from iron. Kaupp proposed that the $[Ru\text{-}L]^{1+}$ ($S = 1/2$) moiety is best described as a superposition of resonance structures $[Ru^{II}\text{-}(L^{\bullet})]^{1+} \leftrightarrow [Ru^{III}\text{-}(L^{2-})]^{1+}$ such that the "true" spectroscopic oxidation state is intermediate between these integer descriptions [29]. Accordingly, the dicationic unit was described as a superposition of the $[Ru^{II}\text{-}(L^{0})]^{2+} \leftrightarrow [Ru^{III}\text{-}(L^{\bullet})]^{2+}$ resonance structures [29]. An XAS study was conducted on $[Ru(cyclam)(tdt)]^{1+}$ ($S = 1/2$) and its one-electron oxidized product, $[Ru(cyclam)(tdt)]^{2+}$ ($S = 0$), which are isoelectronic to the previously described Fe series [30]. The Ru K-edge spectra, whose rising-edge directly respond to the Z_{eff} of the Ru ion, exhibited energies of 22,115.3 eV for $[Ru(cyclam)(tdt)]^{1+}$ and 22,115.6 eV for $[Ru(cyclam)(tdt)]^{2+}$ [30]. These data were calibrated by comparison with the edge position of $[Ru^{II}(cyclam)(dtc)](BPh_4)$ ($S = 0$) and *cis*-$[Ru^{III}(cyclam)Cl_2]Cl$ ($S = 1/2$) at 22,114.6 and 22,115.8 eV, respectively. The shift of 1.2 eV to higher energy for $[Ru^{III}(cyclam)Cl_2]Cl$ supports the assignment that it possesses a bona fide Ru(III) d^5 central ion, whereas $[Ru^{II}(cyclam)(dtc)](BPh_4)$ has a genuine Ru(II) d^6 ion. The result for $[Ru(cyclam)(tdt)]^{1+}$ sits midway between these two edges, and highlights the non-integer spectroscopic oxidation state for the Ru ion. For $[Ru(cyclam)(tdt)]^{2+}$, the value is high enough that the Ru ion could be defined with a physical oxidation state of +III.

An overlay of the S K-edge spectra of $[Ru(cyclam)(tdt)]^{1+/2+}$ is provided in Fig. 9 [30]. A low-energy pre-edge peak at 2470.0 eV is evident and bears some resemblance to the radical fingerprint peak in $[Fe^{III}(cyclam)(tdt^{\bullet})]^{2+}$. This feature is described as a S $1s \rightarrow$ SOMO transition for $[Ru(cyclam)(tdt)]^{1+}$ where the SOMO comprises 34.9% Ru d_{xz} and 56.6% tdt π^*; the remainder is found on the cyclam unit. So, in many respects, this is our fingerprint peak since the SOMO possess considerable ligand radical character with contributions from the $[Ru^{III}(cyclam)(tdt^{\bullet})]^{1+}$ resonance structure, however, unlike the iron analogue, the unpaired spin is truly delocalized (Class III) over both metal and ligand.

The S K-edge spectrum of $[Ru(cyclam)(tdt)]^{2+}$ has a very intense pre-edge peak at the same energy (2469.9 eV) as for the monocation. This indicates that oxidation of the latter involved removing the electron from the heavily delocalized SOMO without dramatically altering its composition (27.1% Ru; 61.2% tdt), thus a delocalized LUMO is created. Therefore, the electronic structure is best represented by the resonance structures $\{[Ru^{II}(cyclam)(tdt^{0})]^{2+} \leftrightarrow [Ru^{III}(cyclam)(tdt^{\bullet})]^{2+} \leftrightarrow [Ru^{IV}(cyclam)(tdt^{2-})]^{2+}\}$. Given their apparent equal weighting, the effective average oxidation state for the Ru ion is +III, in keeping with the rising-edge energy in the Ru K-edge. These observations were corroborated by TD-DFT calculations.

The outcome facilitated a detailed comparison of the electronic structures of three isoelectronic species, namely $[Co^{III}(tren)(bdt^{\bullet})]^{2+}$, $[Fe^{III}(cyclam)(tdt)]^{1+}$, and $[Ru(cyclam)(tdt)]^{1+}$. All possess a doublet ground state, though this manifests in distinctly different ways: $[Co^{III}(tren)(bdt^{\bullet})]^{2+}$ has a diamagnetic Co(III) d^6 ($S_{Co} = 0$) ion bound by a dithiolene ligand radical ($S_L = 1/2$); $[Fe^{III}(cyclam)(tdt)]^{1+}$ is a Werner-type complex with a low-spin ferric d^5 configuration; and finally the SOMO of $[Ru(cyclam)(tdt)]^{1+}$ is completely delocalized represented by two resonance structures $\{[Ru^{II}(cyclam)(tdt^{\bullet})]^{1+} \leftrightarrow [Ru^{III}(cyclam)(tdt)]^{1+}\}$. This behavior is a consequence of the relative energies of the metal d orbitals with respect to the redox-active π^* orbital of the dithiolene ligand, as depicted by the simplified bonding scheme in Fig. 10. The energy of the Fe 3d orbitals is higher than the dithiolene ligand π donor orbitals giving rise to a "normal" bonding situation (see Section 4.1). The corresponding Co complex exhibits the lowest d orbital energies because of the greater effective nuclear charge of what is formally low-spin Co(IV) d^5. This facilitates an "inverted" bonding scheme (Fig. 12, Section 4.1) the consequence of which is that one electron is transferred to Co from the dithiolate ligand generating the coordinated dithiolene π radical monoanion. The Ru 4d orbitals are equivalent in energy to the ligand π donor orbitals and therefore adopt a completely covalent bonding situation; the assignment of an integer physical oxidation state is no longer meaningful.

The pervasive covalency persists in $[Ru(cyclam)(tdt)]^{2+}$ such that its closed-shell singlet ground state is best viewed by three resonance structures $\{[Ru^{II}(cyclam)(tdt^{0})]^{2+} \leftrightarrow [Ru^{III}(cyclam)(tdt^{\bullet})]^{2+} \leftrightarrow [Ru^{IV}(cyclam)(tdt^{2-})]^{2+}\}$.
The analogous Fe compound is a singlet diradical with strongly antiferromagnetic coupled metal- and ligand-centered unpaired electrons, $[Fe^{III}(cyclam)(tdt^{\bullet})]^{2+}$.

4. Bis(dithiolene) complexes

The decades old debate regarding the correct electronic structure description for transition metal bis(dithiolene) complexes was revived with three pivotal XAS studies [31–33]. Specifically, sulfur

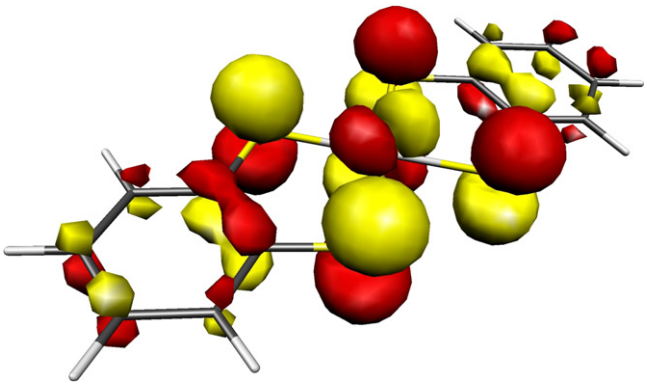

Fig. 11. Depiction of the redox-active $2b_{2g}$ MO in square planar bis(dithiolene) complexes [17].

K-edge XAS, as a direct probe of the sulfur 3p content of the half and unoccupied orbitals, did more than any other spectroscopic venture, reveal the underlying noninnocence of dithiolene ligands. The conclusions drawn were complimented by measurements of various metal K- and L-edges, and tidily wrapped up by theoretical calculations.

Before going to the actual complexes, it is instructive to have an idea about the electronic structure of the hypothetical bis(dithiolato) ligand unit $(L_2)^{4-}$ [17,33,34]. The ligand unit of D_{2h} symmetry features eight orbitals corresponding to symmetry-adapted linear combinations of the sulfur 3p orbitals. Four of these are of π-type ($1b_{3g}$, $1b_{1u}$, $1b_{2g}$, $1a_u$) and the remaining four are of σ-type orbitals ($1b_{2u}$, $1b_{3u}$, $1b_{1g}$, $1a_g$). For the hypothetical bis(dithiolato) unit, the HOMO (π^*-b_{2g}) can undergo a symmetry-allowed π interaction with a d_{xz} orbital of a central metal ion. Similarly, the symmetric and antisymmetric combinations of the bis(dithiolato) $1a_u$ and $1b_{3g}$ orbitals, respectively, can π-interact with the d_{yz} metal orbital. Finally, the antisymmetric $1b_{1g}$ orbital can σ-interact with the metal d_{xy} orbital. Members of any one electron transfer series (except Cu) were found to differ by the occupation of the redox-active $2b_{2g}$ MO (Fig. 11). As it will be shown, the innocent and noninnocent nature of the dithiolene ligand in a bis(dithiolato) ligand unit is controlled mainly be the extent of interaction of the ligand π^*-b_{2g} orbital with the metal d_{xz} orbital, in turn dictated by their relative energies.

The $2b_{2g}$ MO is filled in dianionic bis(dithiolene) complexes of Ni, Pd, Pt, and the monoanionic Cu and Au species. It is the SOMO in the one-electron oxidized product, the spin doublet $[M(L)_2]^{1-}$ (M = Ni, Pd, Pt) and $[Au(L)_2]^0$ whose composition has been extensively studied by EPR [4,14] and ESEEM/ENDOR [35] spectroscopies that led to the conclusion that it is predominantly ligand in character with varying degrees of metal (d_{xz}) content. These EPR results would be utilized to calibrate and interpret the S K-edge data. A further one-electron oxidation to diamagnetic neutral Ni, Pd, Pt, and monocationic Au complexes results in emptying the $2b_{2g}$ MO such that it is now the LUMO. Using S K-pre-edge peak intensities and theoretical calculations, the sulfur 3p content, and thus the covalency in bis(dithiolene) complexes was resolved and the ground state wavefunction described.

4.1. Nickel, palladium, and platinum

Solomon and co-workers first addressed the bonding and covalency in the bis(dithiolene)nickel series in 2003, with an elaborate sulfur K-edge XAS and density functional theoretical study [33]. The compounds in question, $[Ni(mdt)_2]^z$ ($z = 0, 1-, 2-$), had been crystallographically, spectroscopically and theoretically characterized a few years earlier by Holm [16]. The noninnocence of the dithiolene ligand had already been exposed by EPR [4,14] and ENDOR/ESEEM [35] spectroscopies, however, that examination was limited to the paramagnetic member of the series, the $S = 1/2$ monoanion. Sulfur K-edge XAS, complimented by Ni K- and L-edge XAS, and calibrated by EPR data for the monoanion, would deliver a quantitative assessment of the bonding and covalency across the whole series.

Covalency was defined as the ligand (sulfur) character in the unoccupied orbital $\varphi^* = (1-\alpha^2)^{1/2}|\text{metal 3d}\rangle - \alpha|\text{S 3p}\rangle$ [22,36]. The sulfur covalency is determined from the intensity of the transition (D_0) to an unoccupied orbital (φ^*) by the relationship detailed in Eq. (1), where the α^2 is the S 3p content, A the area under the pre-edge peak, n the number of absorbing nuclei ($n = 4$ for bis(dithiolene) complexes). The key ingredient is the transition dipole integral, I(S), for the S $1s \rightarrow 3p$ excitation [21], which is derived from the experimental spectrum.

$$D_0(S\,1s \rightarrow \varphi^*) = \text{constant}|\langle S\,1s|\mathbf{r}|\varphi^*\rangle|^2 = \alpha^2 I(S\,1s \rightarrow 3p) = \left(\frac{A}{3n}\right)\alpha^2 I(S) \quad (1)$$

The poignant questioned raised in this study was the notion of an "inverted bonding" scheme. A "normal bonding" scheme (Fig. 12, left) is characterized as having the metal d orbital manifold destabilized relative to the ligand orbitals; an inverted arrangement (Fig. 12, right) is, not surprisingly, the other way round. If the ligand content exceeds 50%, this is the territory of the inverted scheme and underscores a highly covalent bonding scenario.

Solomon and co-workers set about defining the transition dipole integral, I(S) for the free dithiolene ligand, approximating it via a linear relationship between I(S) and the effective nuclear charge (Z_{eff}) of sulfur. This came about based on determined integrals for sulfide (S^{2-}) [37] and thiolate (RS^-) [38], and merely extrapolating the value for Na_2edt based on a comparison of their rising-edge energies ascribed as the S $1s \rightarrow 4p$ transition from recorded S K-edge spectra of these salts [33]. A value of I(S) = 9.15 was obtained. The consequence of having two dithiolene ligands in proximity in

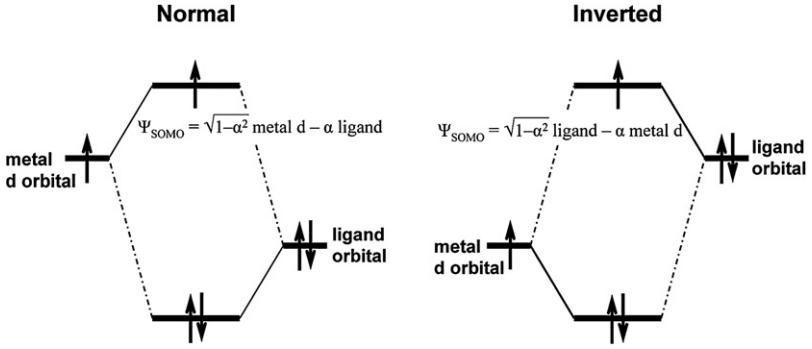

Fig. 12. Depiction of the relative orbital energies that generate a normal (left) and inverted (right) bonding scheme [33].

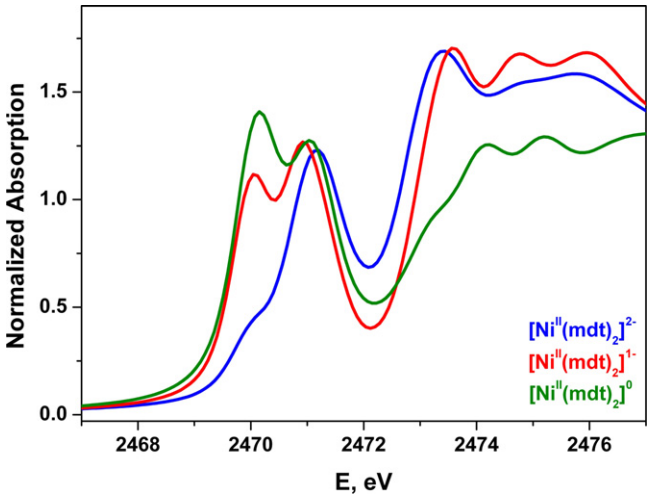

Fig. 13. Comparison of the normalized S K-edge XAS spectra for $[Ni(mdt)_2]^z$ ($z = 0, 1-, 2-$) [33].

a square planar (D_{2h} symmetry) arrangement, as well as the inclusion of a Ni ion, further modified the $I(S)$ value: extrapolation gave 9.84, 10.39, and 10.94, for the dianionic, monoanionic, and neutral species, respectively. This was tracked by the S 1s → C–S π* transition in the S K-edge spectra. The spectra themselves, overlaid in Fig. 13, show two pre-edge peaks. For the dianion, the first low-energy shoulder arises from ~20% oxidized impurity in this highly air-sensitive compound; subtraction of the spectrum of the monoanion eliminated this feature, leaving one pre-edge peak at 2471.2 eV.

The spectra of the monoanion and neutral complexes have two pre-edge peaks at 2470.0 and 2471.0 eV, and 2470.1 and 2471.1 eV, respectively. Pseudo-Voigt deconvolution provided a value for D_0 which in turn produced quantified covalencies for the frontier orbitals (α^{2c}, Table 1). Reassuringly, the numbers resemble a similar determination by EPR (averaged for the monoanion α^{2b}, Table 1). The data experimentally confirm the inverted bonding scheme, with frontier σ* $1b_{1g}$ (Ni $d_{x^2-y^2}$ + Lσ* − b_{1g}; $13b_{1g}$ in Ref. [33]) and π* $2b_{2g}$ (Ni d_{xz} + L π* − b_{2g}; $5b_{1g}$ in Ref. [33]) being of predominantly

Table 1
Pre-edge peak energies, identified transition, and experimental covalencies derived from S K-edge pre-edge spectra.

	E (eV)	Transition[a]	Experimental covalency (%)		
			α^{2b}	α^{2c}	α^{2d}
$[Ni(mdt)_2]^{2-}$	2471.2	S 1s → $1b_{1g}$	77	81	62
$[Ni(mdt)_2]^{1-}$	2470.0	S 1s → $2b_{2g}$	59	62	59
	2471.0	S 1s → $1b_{1g}$	71	75	58
$[Ni(mdt)_2]^0$	2470.1	S 1s → $2b_{2g}$	67	70	56
	2471.1	S 1s → $1b_{1g}$	57	57	51

[a] $13b_{1g} = 1b_{1g}$ MO and $5b_{2g} = 2b_{2g}$ MO in Ref. [33].
[b] XAS and EPR covalency values averaged for $[Ni(mdt)_2]^{1-}$ complex from Ref. [33].
[c] Quantification based on old transition dipole integral from Ref. [33].
[d] Quantification based on new transition dipole integral from Ref. [32].

ligand character [33]. The Ni d_{yz}, d_{z^2}, and $d_{x^2-y^2}$ have no involvement in bonding and are occupied across the series; the MO scheme for this three-membered series is presented in Fig. 14. The S 3p character (EPR calibrated, α^{2b}, Table 1) of the $1b_{1g}$ MO decreases along the series, with 77% for the dianion, 71% for the monoanion, and 57% in the neutral complex (Table 1). The opposite behavior occurs for the $2b_{2g}$ MO, with 59% S 3p in the monoanion that increases to 67% in the neutral.

Furthermore, Solomon et al. then calibrated their DFT calculations to match the experimental covalencies. The GGA density functional calculations worked best with 10% Hartree–Fock exchange that satisfactorily accounted for the S 3p covalency in the $2b_{2g}$ LUMO of $[Ni(mdt)_2]^0$. This, however, led to no spin polarization of the ground state – a broken symmetry solution with spin of different sign on each ligand [19,33]. When the Hartree–Fock exchange was dialed up to 25%, 0.4 of an electron spin was located on each ligand. The latter solution was in better agreement with the EPR-calibrated data (based on EPR spin distribution [14,35]) displayed in Table 1. The 25% Ni d_{xz} character of the $2b_{2g}$ LUMO of $[Ni(mdt)_2]^0$ acts as a superexchange pathway between the two partially spin polarized ligands [17,33].

The accuracy of the extrapolated $I(S)$ values for coordinated dithiolene ligands was improved with correlation of the S K-edge XAS data with the ^{33}S EPR superhyperfine for $[Cu^{II}(mnt)_2]^{2-}$ [32]. The value of $I(S) = 14.1$ for the S 1s → 3p transition in this complex represents a S atom with considerably more positive charge

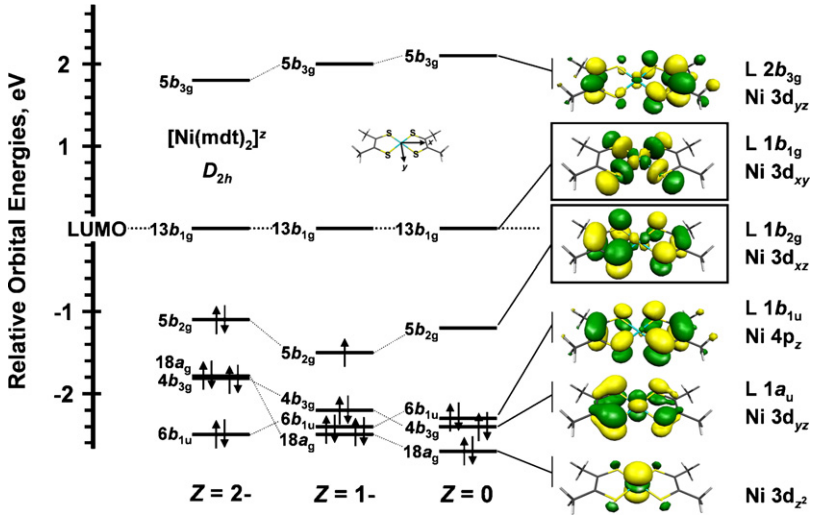

Fig. 14. Kohn-Sham orbital picture of the $[Ni(mdt)_2]^z$ ($z = 0, 1-, 2-$) series with symmetrized geometry from the X-ray structure of $[Ni(mdt)_2]^0$ calculated at the B88P86/BS5 level [33].

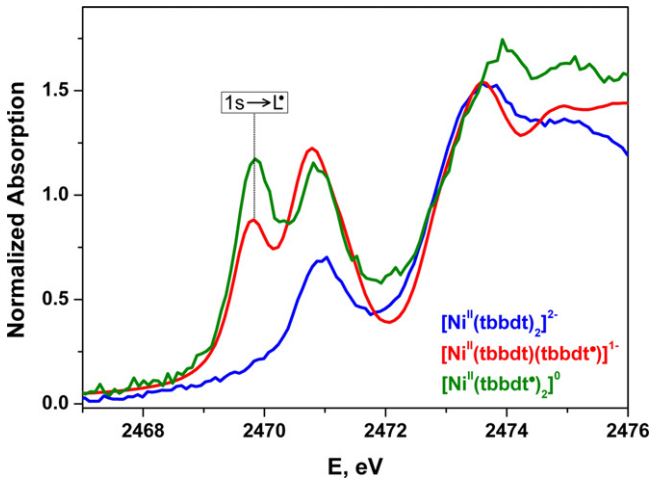

Fig. 15. Comparison of the normalized S K-edge XAS spectra for $[Ni(tbbdt)_2]^z$ ($z = 0, 1-, 2-$) [31].

than the previous S^{2-} and RS^- benchmarks [33], and thereby a more accurate linear relationship between $I(S)$ and the S 1s → 4p transition energy was derived such that the $I(S)$ for a range of S-containing ligands could be determined by *interpolation* rather than *extrapolation*. The result was a revision of the covalencies for the $[Ni(mdt)_2]^{0/1-/2-}$ series as noted in Table 1 (α^{2d}), and a comparison with the $[Ni(mnt)_2]^{1-/2-}$, bearing the more electron withdrawing cyanide substituents on the dithiolene ligand.

The final revision of the experimental and calculated covalency in the bis(dithiolene)nickel series came from a further re-evaluation of the S 1s → 3p transition dipole integral [31]. It had long been known that the magnitude of the integral is dependent on the radial functions of the 1s and 3p orbitals, and in the case of the latter that are involved in bonding, these orbitals will exhibit different degrees of radial distortion (as an expansion in the case of antibonding orbitals) depending on whether the acceptor orbital with S 3p character is σ* or π*. The pre-edge transitions for these bis(dithiolene) complexes are S 1s → $1b_{1g}$ σ* and S 1s → $2b_{2g}$ π*, and it was shown that the π* orbital is more contracted than the σ* orbital giving (up to 20%) a smaller value for the dipole integral. The S K-edge XAS data collected for the $[Ni(tbbdt)_2]^{0/1-/2-}$ series is shown in Fig. 15, and are very similar to both $[Ni(mdt)_2]^{0/1-/2-}$ [33] and $[Ni(mnt)_2]^{1-/2-}$ series [32].

The salient point of this work was the fact that neither $I(S)$ nor α^2 are physical observables, whereas the oscillator strength *is* an observable. Therefore, the oscillator strength was directly calculated using a newly devised time dependent (TD) DFT protocol [31], and then $I(S)$ and α^2 were factorized out after the correlation of experimental and calculated oscillator strengths, using $[Au^{III}(tbbdt)(tbbdt^{\bullet})]^0$ as the reference complex (*vide infra*). The results for a range of bis(dithiolene) compounds studied are posted in Table 2, including a redetermination of the covalency in $[Ni(mdt)_2]^{1-/2-}$.

Fig. 16 presents an overlay of the S K-edge XAS spectra for the bis(dithiolene) monoanions of Ni, Pd and Pt [31]. Each exhibit two pre-edge peaks with the lowest energy feature (2469.7 ± 0.2 eV) assigned as the S 1s → $2b_{2g}$ transition – our radical fingerprint – with one hole in this predominantly ligand-based orbital (>50%, Table 2). The second and more intense peak is the 1s → $1b_{1g}$ transition that increases in intensity and shifts ~1.5 eV to higher energy on going from $[Ni(tbbdt)_2]^{1-}$ to $[Pd(tbbdt)_2]^{1-}$ to $[Pt(tbbdt)_2]^{1-}$.

Therefore, it has been ultimately shown through S K-edge XAS measurements that bis(dithiolene) complexes of Group 10 metals (Ni, Pd, Pt) form three-membered electron transfer series that are interrelated by ligand-centered redox events while the metal maintains a +II physical oxidation state throughout (Scheme 5).

Table 2
Calculated and experimental covalencies for bis(dithiolene) complexes [31].

Complex	Transitions	Experimental covalency[a]	Calculated covalency
$[Ni(tbbdt)_2]^{1-}$	S 1s → $2b_{2g}$	53.6	47.9
	S 1s → $1b_{1g}$	76.8	84.6
$[Pd(tbbdt)_2]^{1-}$	S 1s → $2b_{2g}$	61.1	56.0
	S 1s → $1b_{1g}$	81.8	94.0
$[Pt(tbbdt)_2]^{1-}$	S 1s → $2b_{2g}$	56.2	56.7
	S 1s → $1b_{1g}$	86.0	82.0
$[Au(tbbdt)_2]^0$	S 1s → $2b_{2g}$	60.0	60.0
	S 1s → $1b_{1g}$	110.0	110.0
$[Au(tbbdt)_2]^{1-}$	S 1s → $1b_{1g}$	133.2	109.2
$[Cu(tbbdt)_2]^{1-}$	S 1s → $1b_{1g}$	107.1	115.2
$[Ni(tbbdt)_2]^{2-}$	S 1s → $1b_{1g}$	45.9	77.6
$[Ni(tbbdt)_2]^0$	S 1s → $2b_{2g}$	76.7	[b]
	S 1s → $1b_{1g}$	74.0	
$[Pd(tbbdt)_2]^{2-}$	S 1s → $1b_{1g}$	[c]	88.2
$[Pt(tbbdt)_2]^{2-}$	S 1s → $1b_{1g}$	[c]	83.1
$[Co(tbbdt)_2]^{1-}$	S 1s → $2b_{3g}$	56.1	52.5
	S 1s → $2b_{2g}$		
	S 1s → $1b_{1g}$	81.8	80.0
$[Ni(mdt)_2]^{1-}$	S 1s → $2b_{2g}$[d]	46.2	51.2
	S 1s → $1b_{1g}$[e]	91.2	83.4
$[Ni(mdt)_2]^{2-}$	S 1s → $1b_{1g}$	93.0	76.8

[a] Neutral $[Au(tbbdt)_2]^0$ calibrated experimental covalency.
[b] Calculations were not performed.
[c] Feature is not well resolved from edge and therefore accurate areas (covalencies) cannot be obtained.
[d] Equivalent to the S 1s → $5b_{2g}$ transition in Ref. [33].
[e] Equivalent to the S 1s → $13b_{1g}$ transition in Ref. [33].

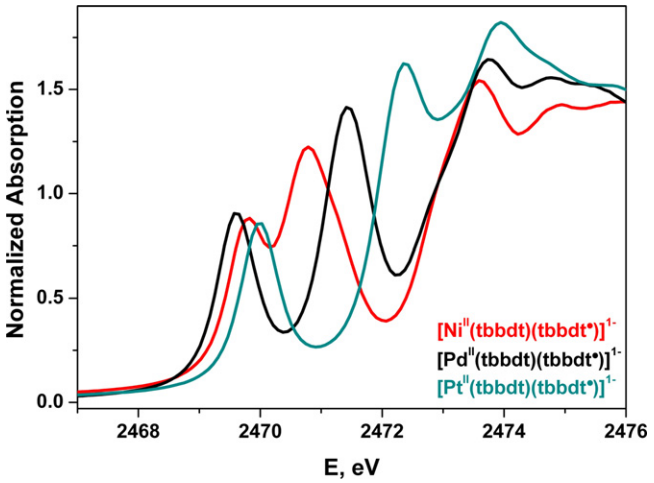

Fig. 16. Overlay of the normalized S K-edge XAS spectra for $[M(tbbdt)_2]^{1-}$ (M = Ni, Pd, Pt) [31].

4.2. Copper and gold

A single crystal of 0.1–0.5 mol% $(NBu_4)_2[Cu^{II}(mnt)_2]$ ($S = 1/2$) diluted in diamagnetic $(NBu_4)_2[Ni^{II}(mnt)_2]$ was analyzed by X-band EPR spectroscopy [40]. Due to the sample being a selectively orientated crystal, the extremely narrow spectral line width allows for observation of ^{33}S magnetic hyperfine features [40,41]. From

$$[M^{II}(L^{\bullet})_2]^0 \underset{-e}{\overset{+e}{\rightleftharpoons}} [M^{II}(L)(L^{\bullet})]^{1-} \underset{-e}{\overset{+e}{\rightleftharpoons}} [M^{II}(L)_2]^{2-}$$
$$(S = 0) \qquad (S = {}^1/_2) \qquad (S = 0)$$

Scheme 5. Three-membered electron transfer series for $[M(L)_2]^0$ (M = Ni, Pd, Pt) [39].

$$[Au^{III}(L^{\bullet})_2]^{1+} \underset{-e}{\overset{+e}{\rightleftharpoons}} [Au^{III}(L)(L^{\bullet})]^{0} \underset{-e}{\overset{+e}{\rightleftharpoons}} [Au^{III}(L)_2]^{1-} \underset{-e}{\overset{+e}{\rightleftharpoons}} [Au^{II}(L)_2]^{2-}$$
$$(S=0) \qquad (S=1/2) \qquad (S=0) \qquad (S=1/2)$$

Scheme 6. Four-membered electron transfer series for $[Au(L)_2]^z$ (z = 1+, 0, 1−, 2−) [39,45].

this EPR spectrum, the sulfur content of the SOMO was determined which led to a reappraisal of the dipole integral, $I(S)$, for the S 1s → 3p transition in $[Cu^{II}(mnt)_2]^{2-}$ (S = 1/2) [32]. Solomon et al. then used this $I(S)$ value to compute the covalency in $[Cu(mnt)_2]^{1-/2-}$. The S K-edge spectra are characterized by one pre-edge feature, at 2470.1 eV and 2470.4 eV, respectively. The intensity is significantly greater for the monoanionic complex. The dianion is readily described as a classic Werner-type complex with a Cu(II) d^9 central ion coordinated by two dianionic dithiolate ligands. This assignment was provided by the axial EPR spectrum that is the hallmark of Cu(II) [4]. Thus, the pre-edge peak arises from the S 1s → $1b_{1g}$ transition; the σ* SOMO of this dianion. The one-electron oxidized product, $[Cu^{III}(mnt)_2]^{1-}$ (S = 0) was classified as a metal-centered event, giving a Cu(III) d^8 central ion with two dithiolate ligands, as opposed to a Cu^{II}-radical species proposed by Sawyer et al. [42]. The shift to lower energy by 0.3 eV reflects an increase in Z_{eff} of the metal ion that stabilizes the frontier orbitals with respect to the S 1s orbital. The calculated per hole (one hole for the dianion and two holes in the monoanion) S character is 0.7 in $[Cu^{III}(mnt)_2]^{1-}$ compared to 0.63 in $[Cu^{II}(mnt)_2]^{2-}$. This was corroborated by Cu K- and L-edge with measurements, where the pre-edge energies shift by ∼1.5 eV upon one-electron oxidation of $[Cu^{II}(mnt)_2]^{2-}$ to $[Cu^{III}(mnt)_2]^{1-}$ [32].

For its Group 11 congener, bis(dithiolene)gold complexes have been investigated in depth in the past [43]. Most are monoanionic $[Au^{III}(L)_2]^{1-}$ (S = 0) where the diamagnetic Au(III) d^8 central ion is coordinated by two dianionic dithiolate ligands. Like so many other dithiolene compounds, this also exhibited reversible one-electron redox chemistry, and formed three-membered electron transfer series with an aryl dithiolene. It was the isolation and characterization of the neutral species, $[Au^{III}(tbbdt)(tbbdt^{\bullet})]^{0}$ (S = 1/2) that showed the oxidation was ligand-centered [44]. Most insightful were the ^{197}Au Mössbauer spectral parameters, with the isomer shift δ = 3.36 mm s^{-1} and quadrupole splitting ΔE_Q = 2.92 mm s^{-1} for $[Au^{III}(tbbdt)_2]^{1-}$ remaining more or less unchanged in the neutral compound, with δ = 3.20 mm s^{-1} and ΔE_Q = 3.06 mm s^{-1} [44].

The electron transfer series was extended to four members using a substituted 1,2-diphenyl-1,2-dithiolate ligand $(pdt)^{2-}$ [45]. The structural characterization of the neutral and monocationic complexes showed shortening of the C–S bonds and concomitant lengthening of the olefinic C–C bonds as the species became more oxidized. The electronic structures of the members of this series are defined in Scheme 6. The electronic absorption spectra displayed characteristics of S,S′-coordinated dithiolene radicals with intervalence charge transfer (IVCT) bands in the near infrared region of the spectrum, and a truly amazing X-band EPR spectrum for $[Au^{III}(pdt)(pdt^{\bullet})]^{0}$ (S = 1/2), which is only the second example where the quadrupole interaction is larger than the magnetic hyperfine interaction, confirms a d^8 central ion for this compound with a $(1a_g)^2(2a_g)^2(1b_{3g})^2(1b_{2g})_2(1a_u)^2(2b_{3g})^2(1b_{1u})^2(2b_{2g})^1(1b_{1g})^0$ electronic configuration; the MO scheme is displayed in Fig. 17 [17].

The S K-edge XAS spectra of $[Au^{III}(tbbdt)_2]^{0/1-}$ are overlaid in Fig. 18. A single intense peak in the spectrum of $[Au^{III}(tbbdt)_2]^{1-}$ at 2471.18 eV is assigned as the S 1s → $1b_{1g}$ transition. The neutral has an extra pre-edge peak at 2469.8 eV indicating the presence of a ligand radical (S 1s → $2b_{2g}$ transition). Due to the very high effective nuclear charge of gold, the 5d manifold lies very deep in energy, and thus metal-ligand covalency is minimized compared with $[M(L)(L^{\bullet})]^{1-}$ (M = Ni, Pd, Pt) described in Section 4.1. As such, this compound was selected as the reference for TD-DFT computed covalency in the $2b_{2g}$ and $1b_{1g}$ MOs [31], where an integrated area of 0.704 units^2 corresponds to 60% S 3p character in the former;

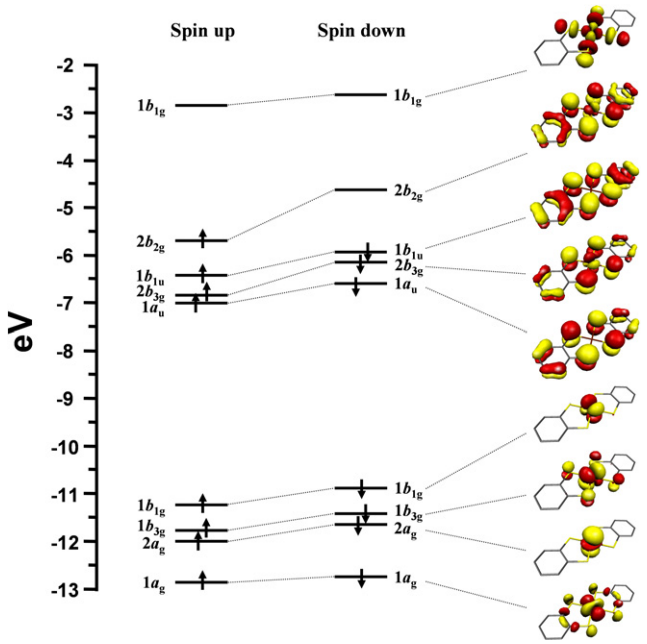

Fig. 17. Kohn-Sham MOs and energy scheme for $[Au^{III}(bdt)(bdt^{\bullet})]^{0}$ from a spin-unrestricted ZORA/B3LYP DFT calculation [17,31].

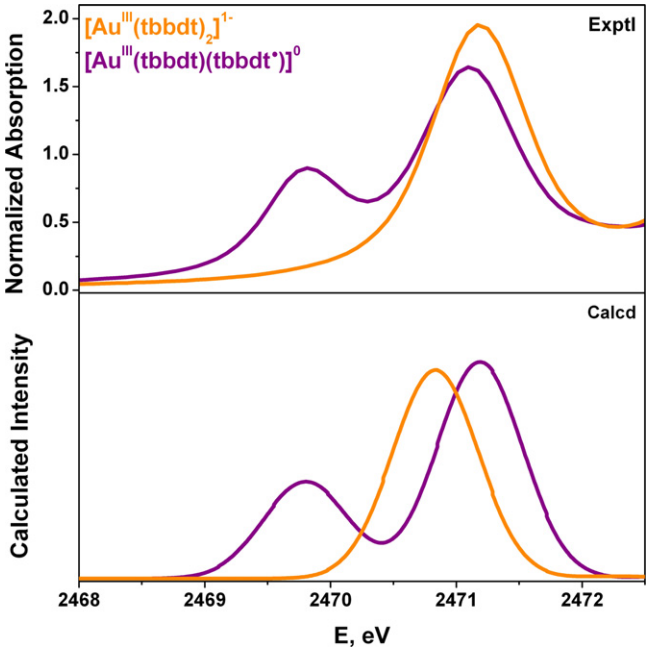

Fig. 18. Experimental (top) and calculated (bottom) S K-pre-edge XAS spectra for $[Au(tbbdt)_2]^{0/1-}$ complexes obtained from ZORA/BP86 TD-DFT calculations [31].

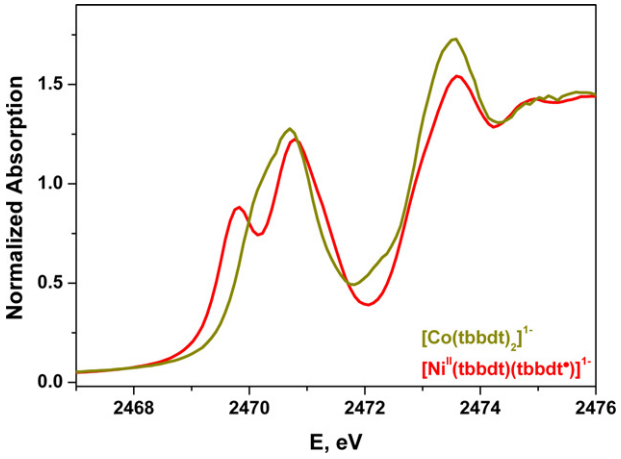

Fig. 19. Overlay of the normalized S K-edge spectra of $[Co(tbbdt)_2]^{1-}$ and $[Ni^{II}(tbbdt)(tbbdt^{\bullet})]^{1-}$ [31].

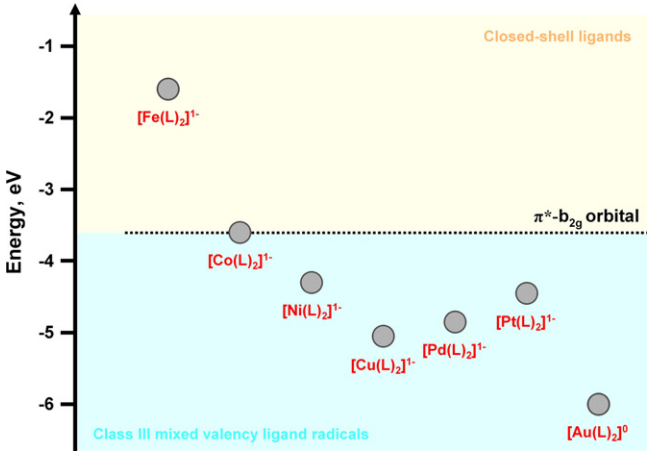

Fig. 20. Calculated energy of the metal d_{xz} orbital relative to the ligand π^*-b_{2g} orbital energy for the different complexes in the $[M(L)_2]^z$ series. Despite the Cu $3d_{xz}$ orbital being lower in energy than the ligand π^*-b_{2g}, the complex is formulated as $[Cu^{III}(L)_2]^{1-}$ with two closed-shell dithiolate ligands (see text) [31].

1.56 units^2 represents 110% S 3p character in the two $1b_{1g}$ holes (Table 2).

The calculated spectra for $[Au^{III}(tbbdt)_2]^{0/1-}$ are compared with the experimental data in Fig. 18, where the calculated transition energies (after a constant shift of +61.22 eV [31]) of 2469.8 and 2471.17 eV for $[Au^{III}(tbbdt)(tbbdt^{\bullet})]^0$ (experimental 2469.8 and 2471.12 eV) and 2470.83 eV for $[Au^{III}(tbbdt)_2]^{1-}$ (experimental: 2471.18 eV). Moreover, the calculated intensity ratio of 1:2.25 in the spectrum of the neutral complex was in excellent agreement with the experimental ratio of 1:2.21.

4.3. Cobalt

The mononuclear complex $[Co(tbbdt)_2]^{1-}$ ($S=1$) was synthesized and structurally characterized in 2005. The electronic structure of this species had been the subject of an intense spectroscopic examination, and based on electronic absorption, variable-field variable-temperature magnetic measurements, magnetic circular dichroism (MCD) spectroscopy, and *ab initio* theoretical calculations, the redox-active $2b_{2g}$ MO was estimated to be 50% Co d_{xz} and 50% ligand π^*-b_{2g}. Therefore, the oxidation state of the Co ion (and dithiolene ligands) cannot be unambiguously assigned, leaving the electronic structure best represented by the following resonance forms $\{[Co^{III}(tbbdt)_2]^{1-} \leftrightarrow [Co^{II}(tbbdt^{\bullet})(tbbdt)]^{1-} \leftrightarrow [Co^{II}(tbbdt)(tbbdt^{\bullet})]^{1-}\}$.

Along with the deep blue color that delivers an envelope of intense CT bands between 500 and 700 nm in the electronic spectrum, the S K-edge spectrum also indicates considerable ligand radical character in this compound. The spectrum, overlaid with that of $[Ni^{II}(tbbdt)(tbbdt^{\bullet})]^{1-}$ ($S=1/2$) in Fig. 19, shows two pre-edge features: a shoulder at 2470.16 eV and a peak at 2470.77 eV. The rising-edge (~2473 eV) is slightly lower in energy than that for the Ni compound (~2473.6 eV). The calculated electron configuration of $(1a_u)^2(1b_{1u})^2(2b_{3g})^1(2b_{2g})^1(1b_{1g})^0$ has a spin triplet ground state with one less valence electron than $[Ni^{II}(tbbdt)(tbbdt^{\bullet})]^{1-}$ ($S=1/2$) with an additional hole in the $2b_{3g}$ MO.

The pre-edge region was calculated using three transitions, with the first peak comprising the two $1s \rightarrow \pi^*$ ($2b_{3g}$ and $2b_{2g}$). The combined covalency calculated of 53% (18% $2b_{3g}$, 35% $2b_{2g}$) compares nicely with the 56% S 3p character derived from the experiment. The second peak is solely the $1s \rightarrow 1b_{1g}$ σ^* transition, to the LUMO, with an experimental covalency of 82% that again is in excellent agreement with the calculations (Table 2).

The experimental – particularly S K-edge – and theoretical correlation of covalency in bis(dithiolene) systems led to the conclusion that with more than 50% S 3p character in the redox-active $2b_{2g}$ SOMO in monoanions of Ni, Pd, Pt, and neutral Au compound, these are best viewed as delocalized Class III mixed-valence ligand radicals coordinated to a closed-shell d^8 central ion. The radical character decreases in the order $[Au^{III}(L)_2]^0 \approx [Pd^{II}(L)_2]^{1-} > [Pt^{II}(L)_2]^{1-} > [Ni^{II}(L)_2]^{1-}$, which is attributed to the energy of the d orbitals in relation to the ligand π donor orbitals. This is made clear in Fig. 20 where the calculated energy of the ligand π^*-b_{2g} orbital is compared to the energy of the d_{xz} orbital for different $[M(tbbdt)_2]^z$ complexes (M = Fe, Co, Ni, Cu, Pd, Pt, Au). For Au and Pd, where the d_{xz} orbital is situated at very low energy so that metal-ligand mixing is minimal, provide maximum ligand character (~60% S 3p). This is contrasted by $[Co(tbbdt)_2]^{1-}$, where the d_{xz} orbital is of comparable energy to the ligand π^*-b_{2g} orbital that maximizes metal-ligand mixing in the $2b_{2g}$ SOMO (35% S 3p). For $[Fe^{II}(tbbdt)_2]^{2-}$ ($S=1$), based on previous work, the first redox event is a metal-centered oxidation because the Fe 3d manifold is much higher in energy than the ligand π-donor orbitals. The only reason why the redox chemistry does not occur in the case of $[Cu^{III}(tbbdt)_2]^{1-}$ ($S=0$) is the electron count – the acceptor d_{xz} orbital is filled in the case of Cu(III) and the only possible acceptor orbital at the copper atom is the d_{xy}-based $1b_{1g}$ orbital that is energetically inaccessible. Despite the high Z_{eff} of Cu(III), oxidation of the ligand does not occur.

5. Tris(dithiolene) complexes

Homoleptic coordination complexes with three dithiolene ligands were initially misdiagnosed by Schrauzer et al. [46]. In their original press release, reactions of early transition metals with dithiolene ligand precursors (dithiophosphoric esters) were said to produce bis(dithiolene) entities only, though this was quickly corrected [47]. Unlike their bis(dithiolene) counterparts, experimental research on tris(dithiolene) complexes rapidly declined in the 1970s, and perhaps in part because unlike the nearly perfect square planar homogeneity of the bis(dithiolene) systems, tris(dithiolene) complexes threw up a number of geometric challenges that were difficult to accommodate in a single picture. Namely, X-ray structural studies of $[Re(pdt)_3]^0$ [48], $[Mo(edt)_3]^0$ [49], and $[V(pdt)_3]^0$ [50,51], published in 1965, 1965, and 1966, respectively, were the first coordination compounds with molecular trigonal prismatic geometry, and defied the maxim that 'six-coordinate equals octahedral'. It soon became apparent that there was a sliding scale to the trigonal prismatic geometry, with the early take-home mes-

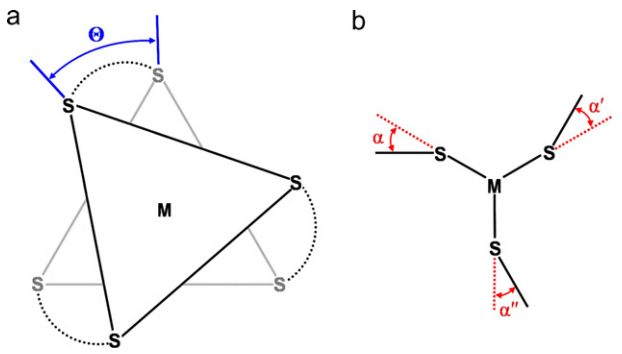

Fig. 21. (a) Trigonal twist angle, Θ, defined as the dihedral angle between the two essentially coplanar S_3 planes of a MS_6 polyhedron, and (b) chelate fold angles, α, α′, α″, defined as the dihedral angle between the MS_2 and S_2C_2 planes along the S···S vector.

sage that the more reduced species drifted toward octahedral but not with any defining regularity [52,53].

The pioneers in this field recognized an intrinsic electronic effect was operative but found formulating a self-consistent picture inhibited by the variety of structural modifications available in tris(dithiolene) systems, through varying degrees of twisting and folding (Fig. 21). Therefore, the lack of definition to the electronic structure of what are anywhere from two- to six-membered electron transfer series has seen tris(dithiolene) complexes largely ignored in contrast to the recent advances in application driven studies employing their bis(dithiolene) analogues [54]. The use of X-ray absorption spectroscopy has been a revelation in this area of research, with the elegant combination of metal and sulfur K-edge studies complementing existing spectroscopic measurements obtained over the last half century.

Tris(dithiolene) complexes are quite different from their bis(dithiolene) counterparts with respect to a ligand field theoretical picture. In general terms, the three-fold axis splits the d orbitals into one nondegenerate a_1 – the nonbonding d_{z^2} orbital – and two sets of degenerate *e* orbitals ($d_{x^2-y^2,xy}$ and $d_{xz,yz}$), that are π and σ antibonding, respectively, to three dithiolene ligands. These symmetry labels apply to molecules of D_3 symmetry, which are all species with twist angles not equal to 0° or 60°. For the latter (Θ = 60°), the structure and thus ligand field splitting is that of an octahedron, however, significant deviations from 60° arise due to the restrictions imposed by the ligand bite angle [55] that leads to a small splitting the essentially t_{2g} orbitals into *a* and *e* levels. Nevertheless, for simplicity, molecules with up to 25° twists are still described as octahedral. For Θ = 0°, the structure has a higher symmetry, that of D_{3h}, although the ligand field splitting is the same, with a_1', e' and e'' levels. As noted previously [56,57], the splitting of the a_1' and e' orbitals decrease as the structure twists toward octahedral, until near to the octahedral limit in complexes of Cr, Mn, and Fe, they are more conveniently described as t_{2g} orbitals [57–59].

More interestingly, trigonal prismatic arrays of three dithiolene ligands act cooperatively. Individually, each dithiolate dianion is a six-electron donor. When these are arranged in a trigonal prism, the HOMO of each ligand form one nondegenerate $2a_2'$ orbital that is nonbonding with respect to the metal, and one degenerate e' level that is strongly π bonded to the metal d orbitals of like symmetry. Thus, oxidative holes are generated when electrons are removed from the a_2' orbital is these systems, and hence we characterize the three dithiolene ligands collectively as $(L_3)^{6-}$, with both the a_2' and e' level occupied; $(L_3)^{5-\bullet}$ where the a_2' is the SOMO and thus the unpaired electron is shared by all three dithiolene ligands; and finally $(L_3)^{4-}$, in which the a_2' level is completely empty (LUMO) accounting for two holes but no unpaired electrons (radicals). This is an important distinction with octahedral tris(dithiolenes), such as the Cr electron transfer series [58,59], and the thoroughly interrogated bis(dithiolene) complexes of late transition metals [17,31–34,44,57–59]. It is also worth considering a further oxidation to $(L_3)^{3-\bullet}$ involves removal of a ligand electron from the e' state generating three oxidative holes though only one unpaired electron ($S_L = 1/2$). The existence of this electron configuration in a trigonal prismatic array is highly unlikely, and as is described below, the ligands lose their interdependency, drift to an octahedral arrangement as $(L^{\bullet})_3$, $S_L = 3/2$; the issue of radical (de)localization is still a matter of debate in such systems.

5.1. Vanadium

The crystal structure of $[V(pdt)_3]^0$ ($S = 1/2$) represented only the third example of a coordination complex with molecular trigonal prismatic geometry [50,51], following hot on the heels of $[Re(pdt)_3]^0$ [48], and $[Mo(edt)_3]^0$ [49]. Synonymous with all known dithiolene complexes, this species could be successively and reversibly one-electron reduced to $[V(pdt)_3]^{1-}$ ($S = 0$) and $[V(pdt)_3]^{2-}$ ($S = 1/2$) [50,60–62]. Kwik and Stiefel had already determined through interpretation of the spin Hamiltonian parameters from a single-crystal EPR examination of $[AsPh_4]_2[V(mnt)_3]$ diluted in diamagnetic $[AsPh_4]_2[Mo(mnt)_3]$ that the ground state for this molecule is $^2A_1$ with the unpaired electron located in the $3a_1'$ MO (the d_{z^2} orbital), i.e. a V(IV) d^1 ion coordinated by three dithiolate(2−) ligands [63]. Furthermore, he recognized that the corresponding neutral complex of this series, having a nearly identical room temperature ERP spectrum, has the same $^2A_1$ ground state and that these two members were differed by two electrons removed from the tris(dithiolene) unit [63]. This was supported by extended Hückel molecular orbital calculations performed several years earlier by Eisenberg published along with the full crystallographic analysis [51]. This conclusion refuted testimony of Davison, Edelstein, Holm, and Maki [60,64], who tendered a V(III) d^2 central ion for the neutral and dianionic complexes citing an extensively delocalized unpaired electron across all three ligands; the ^{51}V hyperfine value being half that for a genuine V(IV) center, using $[V^{IV}O(H_2O)_4]^{2+}$ and $[V^0(bpy)_3]^0$ – as it was then classified – as guides[65]. It should be noted that these were more or less the only vanadium EPR data available at the time.

However, the monoanionic member of this electron transfer series is impervious to scrutiny by EPR, so it remained ill-defined in the literature. Hence, there was no better moment to use XAS to study this series [66]. The V K-edge spectra for $[V(pdt)_3]^0$, $[V(pdt)_3]^{1-}$, and $[V(mnt)_3]^{2-}$ are shown in Fig. 22. Included in this plot is the spectrum of $[V^{III}(dtc)_3]^0$, bearing a genuine V(III) ion while retaining the common VS_6 polyhedron [67]. The pre-edge region (5164–5170 eV, inset Fig. 22) shows peaks derived from V 1s → 3d electric dipole-forbidden, but quadrupole-allowed, are most useful at defining the Z_{eff} of the V ion in each compound. The three tris(dithiolene) complexes have identical pre-edge peaks within experimental error at 5466.9 ± 0.2 eV. Most importantly, the first pre-edge peak in the spectrum of $[V^{III}(dtc)_3]^0$ occurs at 5465.7 eV which is 1 eV *lower* in energy. Clearly, the tris(dithiolene) complexes can be assigned a physical oxidation state of +IV for the vanadium ion. The slight shift to lower energy for the dianion is attributed to its distorted octahedral geometry (Θ = 38°), since the pre-edge is dominated by transitions to the $5e'$ ($d_{x^2-y^2,xy}$) MOs.

Furthermore, the pre-edge intensities differ across the four compounds, with a weak pre-edge for $[V^{III}(dtc)_3]^0$ and $[V^{IV}(mnt)_3]^{2-}$ compared to $[V^{IV}(pdt)_3]^0$ and $[V^{IV}(pdt)_3]^{1-}$. The difference lies in the trigonal twist angle, with the larger twist away from centrosymmetric octahedral facilitating greater V 4p mixing into the $5e'$ MOs. So for trigonal prismatic $[V^{IV}(pdt)_3]^0$ (Θ = 4.6°) and $[V^{IV}(pdt)_3]^{1-}$ (Θ = 0.8°) their pre-edge intensity is 2–3 times larger than for

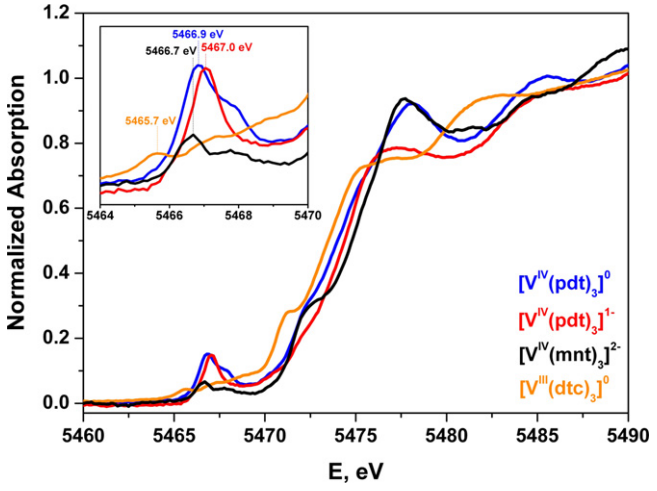

Fig. 22. Comparison of the normalized V K-edge XAS spectra of $[V^{IV}(pdt)_3]^0$, $[V^{IV}(pdt)_3]^{1-}$, $[V^{IV}(mnt)_3]^{2-}$, and $[V^{III}(dtc)_3]^0$. The inset shows an expansion of the pre-edge region [66].

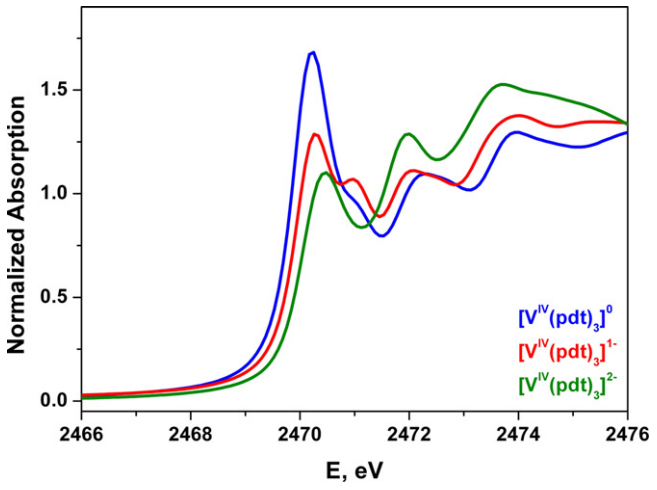

Fig. 23. Comparison of the normalized S K-edge XAS spectra of $[V^{IV}(pdt)_3]^0$, $[V^{IV}(pdt)_3]^{1-}$, and $[V^{IV}(pdt)_3]^{2-}$ [66].

$[V(mnt)_3]^{2-}$ ($\Theta = 38.0^\circ$) with up to 4% V 4p character in the 5e′ level [66]. Moreover, the intensity remains more or less unchanged in the solution spectra, thus proving the trigonal prismatic geometry is retained in the absent of lattice packing forces, and underscoring the versatility of XAS. This useful geometry marker was utilized for electrochemically generated $[V^{IV}(mnt)_3]^{1-}$ ($S = 0$). While the pre-edge peak energy supported a +IV physical oxidation state for the metal ion, the intensity is consistent with a trigonal prismatic structure for this monoanion, as has been revealed for all crystallographically characterized tris(dithiolene) vanadium monoanions [66,68].

In the S K-edge spectra of this series (Fig. 23), the ligand hole peak is clearly evident at 2470.2 eV for $[V(pdt)_3]^0$ and $[V(pdt)_3]^{1-}$, and noticeably absent in the spectrum of $[V(pdt)_3]^{2-}$. It is described as the S 1s → $2a_2'$, transition, to an orbital that is singly occupied in the monoanion, $(L_3)^{5-\bullet}$, and empty for the neutral, $(L_3)^{4-}$. The first pre-edge peak in the dianionic complex, at 2470.4 eV, albeit close in energy to the dithiolene radical peak, is in fact a S 1s → 5e′(α) (α representing a "spin up" electron) that corresponds to the shoulder at 2471.0 eV for $[V(pdt)_3]^{1-}$ and 2471.1 eV for $[V(pdt)_3]^0$; the shift to lower energy consistent with a more reduced tris(dithiolene) ligand set in the dianion, $(L_3)^{6-}$. Additionally, the change in geometry also contributes to the transition energies. The intensity for this peak is a reflection of the S 3p content of the $2a_2'$ and 5e′(α) MOs. The transition to the 5e′(β) (β representing a "spin down" electron) MOs is at higher energy and buried under transitions to the dithiolene C–S π* orbital and the rising edge itself, due to significant spin polarization of the V–S bonds in this series. This is highlighted by the Mulliken spin population analysis, with between 1.4 and 1.5 α-spins on V and significant β-spin on the dithiolene S atoms (Fig. 24).

The crystal structures of all known tris(dithiolene)vanadium monoanions exhibit a significant dithiolene chelate fold angle α >20° (Fig. 21) [66,68]. Although calculations underestimate this in the geometry optimized structures, it does represent a lowering of the symmetry from D_{3h} to C_{3h}. This allows the metal- ($3a_1'$) and ligand-centered ($2a_2'$) SOMOs to mix (since both transform as a') facilitating strong antiferromagnetic coupling giving rise to a diamagnetic ground state that is perhaps the driving force behind the paddle-wheel motif. A synopsis of the electronic structures for this electron transfer series is shown in Fig. 25. The redox-active orbital is the purely ligand-based $2a_2'$ that once filled leads to a distorted octahedral geometry for all structurally characterized dianions. When this orbital is half-filled or empty, the interligand electron repulsion is minimized, and trigonal prismatic VS_6 polyhedra prevail in the neutral and monoanionic species.

5.2. Chromium

Six-coordinate tris(dithiolene)chromium complexes have been known to form a four-membered electron transfer series described by Scheme 7 where each member is related by reversible one-electron transfer waves [53,58,59,61,64,69,70].

This is contrasted by the dioxolene (catechol) [71] and diimine (bipyridine) [72] analogues whose electrochemistry (cyclic voltam-

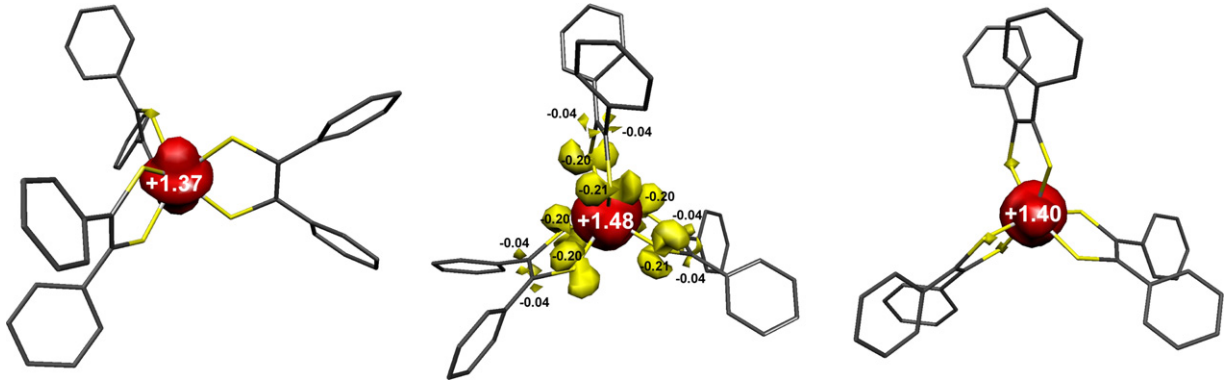

Fig. 24. Mulliken spin density plots for $[V^{IV}(pdt)_3]^0$ (left) and $[V^{IV}(pdt)_3]^{1-}$ (middle) and $[V^{IV}(pdt)_3]^{2-}$ (right) obtained from B3LYP/TZVP DFT calculations [66].

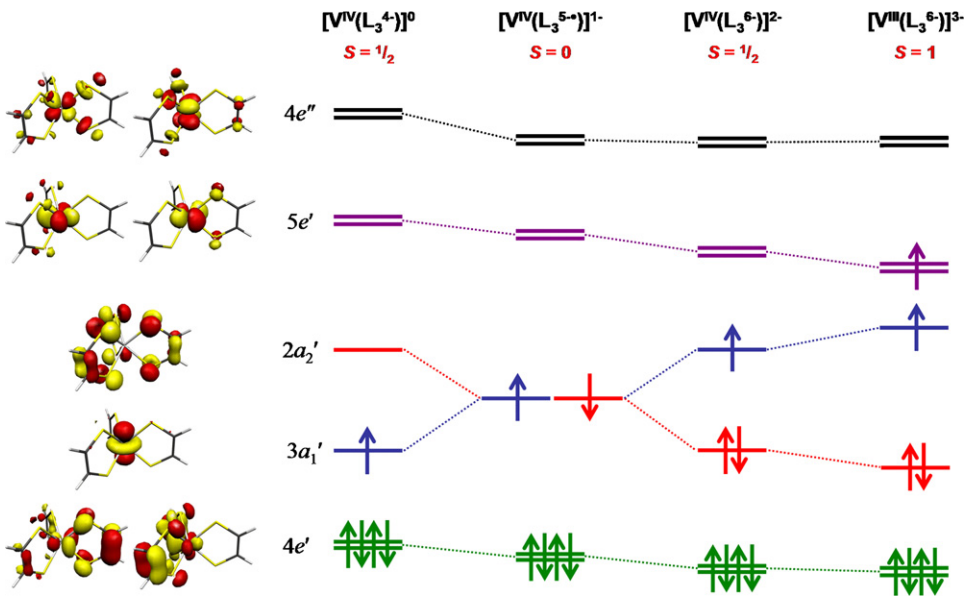

Fig. 25. Qualitative MO scheme depicting the ordering of the frontier orbitals for the $[V(L_3)]^z$ ($z = 0, 1-, 2-, 3-$) electron transfer series derived from B3LYP DFT calculations. The MOs shown left are derived from the calculation of trigonal prismatic $[V(edt)_3]^0$ annotated with D_{3h} symmetry labels [66].

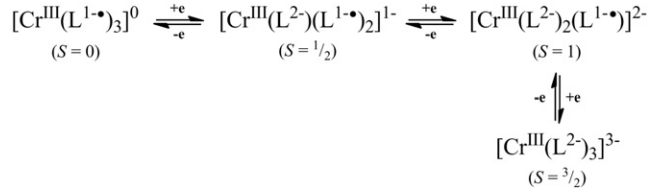

Scheme 7. The four-membered electron transfer series of $[Cr^{III}(L)_3]^z$ ($z = 0, 1-, 2-, 3-$) [58,59].

metry or polarography) extends to all seven members within the solvent window, $[Cr(L)_3]^z$ ($z = 3+, 2+, 1+, 0, 1-, 2-, 3-$). The celebrated work of Raymond et al. [73], and Pierpont et al. [71,74], with input from Kitagawa et al. [75], and calculations by Gordon and Fenske [76], led to a consensus physical oxidation state of +III (d^3) for the Cr ion for the Cr(dioxolene)$_3$ series; each member therefore linked by a ligand-centered one-electron redox process generating *o*-catecholate $(cat)^{2-}$, *o*-benzosemiquinonate $(sq^{\bullet})^{1-}$, and *o*-benzoquinone $(bq)^0$, oxidation levels of the dioxolene ligand, as depicted in Scheme 8.

Therefore, it was rather surprising when in 2006 Lay et al. published an XAS study on Cr-catecholate complexes and argued that the monoanion possessed a Cr(V) d^1 central ion with three closed-shell catecholate(2−) ligands [77]. Similarly, the dianion was diagnosed with a Cr(IV) d^2 ion coordinated by three catecholate(2−) ligands. On the subject of the neutral complex, they were in complete agreement with all another authors and specified a $[Cr^{III}(L^{\bullet})_3]^0$ ($S = 0$) electronic structure, that is a Cr(III) d^3 central ion bound by three open-shell *o*-benzosemiquinonate(1−) ligand radicals. While we could quite spend some time here refuting these observations, we have in fact already addressed this in 2007, showing the overlay of the Cr K-edge XAS spectra of the neutral and monoanionic tris(dioxolene)chromium complexes and revealing both an identical pre- and rising-edge energies [59]. This confirms the early work that both complexes have Cr in the same physical oxidation state (+III). Moreover, this paper also showed the Cr and S K-edge spectra of $[Cr(tbbdt)_3]^{1-}$ ($S = 1/2$), where $(tbbdt)^{2-}$ = 3,5-di-*tert*-butylbenzene-1,2-dithiolate. Arguably, the redox noninnocence of dithiolene ligands bound to Cr had been exposed by electronic absorption and, more importantly, infrared spectroscopy, which indicated the tris(dithiolene) series mirrored the tris(dioxolene) one. This compound was formulated $[Cr^{III}(tbbdt)(tbbdt^{\bullet})_2]^{1-}$ and exhibited two pre-edge peaks in its S K-edge spectrum (Fig. 26). The first at 2469.8 eV is the radical fingerprint assigned as a S 1s → L• transition to the two bonafide holes in the S 3p orbitals. The higher energy feature at 2471.2 eV corresponded nicely to the single intense pre-edge peak at 2470.8 eV in isoelectronic $[Mo^{V}(tbbdt)_3]^{1-}$ ($S = 1/2$),– a transition typical for S,S′-coordinated, closed-shell benzene-1,2-dithiolates(2−) [78].

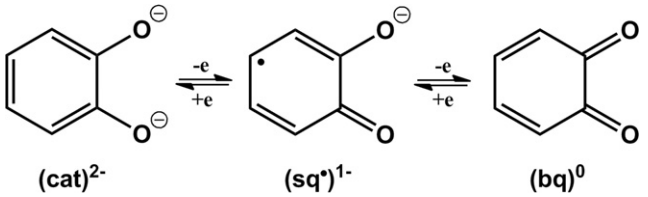

Scheme 8. Dioxolene ligand redox levels [25].

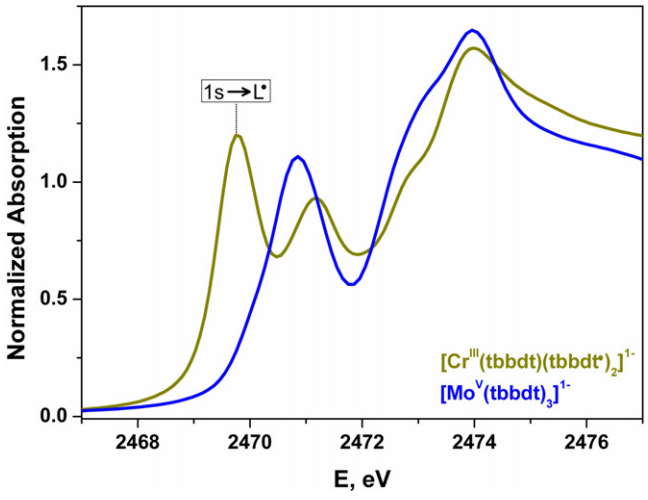

Fig. 26. Comparison of the normalized S K-edge XAS spectra of $[Cr^{III}(tbbdt)(tbbdt^{\bullet})_2]^{1-}$ and $[Mo^{V}(tbbdt)_3]^{1-}$ [59].

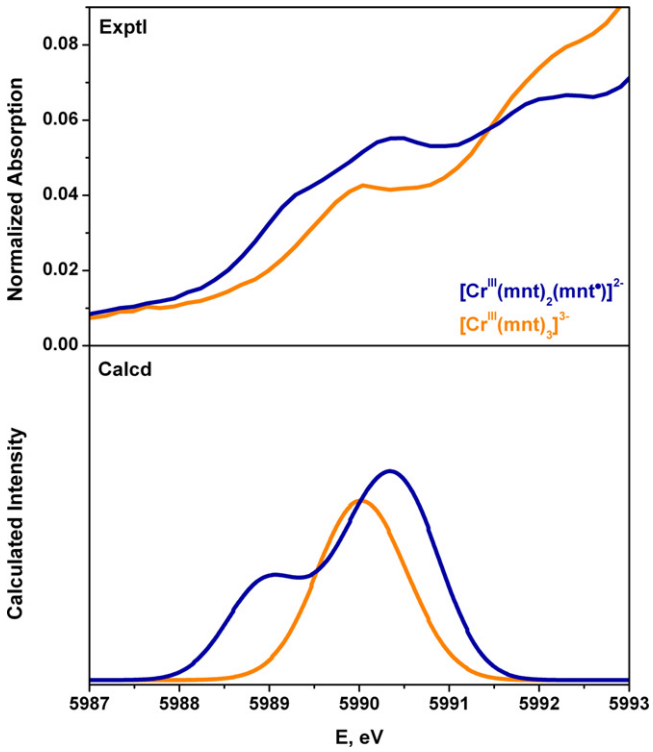

Fig. 27. Experimental (top) and calculated (bottom) Cr K-pre-edge XAS spectra of $[Cr^{III}(mnt)_2(mnt^{\bullet})]^{2-}$ and $[Cr^{III}(mnt)_2]^{3-}$ obtained from BP86 TD-DFT calculations. Calculated intensity in arbitrary units [58].

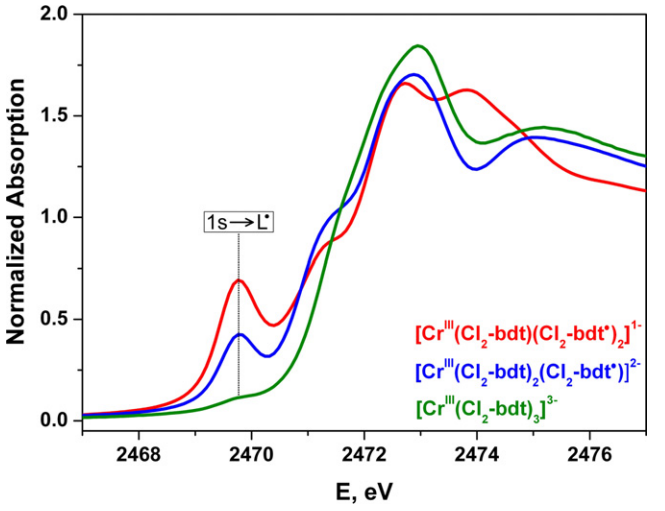

Fig. 28. Overlay of the S K-edge XAS spectra for $[Cr^{III}(Cl_2\text{-bdt})_3]^z$ ($z = 1-, 2-, 3-$) electron transfer series [58].

This was followed by a more complete study of three members of the series: $[Cr(Cl_2\text{-bdt})_3]^z$ ($z = 1-, 2-, 3-$) [58]. Being a symmetrically substituted aromatic dithiolate ligand, it was not amenable to an IR spectroscopic diagnosis, so XAS proved to be the most meaningful experiment. The Cr K-pre-edge energies, that arise from quadrupole-allowed transitions into the 3d manifold that gain intensity from mixing of Cr 4p character, were found to be identical within experimental error at 5990.1 ± 0.2 eV consistent with no change in Z_{eff} across this series. The pre-edge peak for $[Cr^{III}(tbbdt)(tbbdt^{\bullet})_2]^{1-}$ was found at 5989.7 eV; the subtle difference reflecting the varying electronic properties of a ^{t}Bu versus a Cl substituent. Two pre-edge peaks were found in the Cr K-edge spectra of $[Cr(mnt)_3]^{2-}$ ($S = 1$) and $[Cr(mnt)_3]^{3-}$ ($S = 3/2$), with a rather noticeable low-energy shoulder in the former at 5989.4 eV. For the first time these pre-edge peaks were assigned with the aid of TD-DFT calculations. The calculated pre-edges of $[Cr(mnt)_3]^{2-}$ and $[Cr(mnt)_3]^{3-}$ are displayed in Fig. 27, since these are a little more lively than their $[Cr(Cl_2\text{-bdt})_3]^z$ ($z = 1-, 2-, 3-$) counterparts.

For the Werner-type $[Cr^{III}(mnt)_3]^{3-}$, one pre-edge peak assigned as predominately due to the Cr $1s \rightarrow t_{2g}(\beta)$ transitions, that is, excitation to the three singly occupied Cr t_{2g} orbitals. The spectrum of $[Cr(mnt)_3]^{2-}$ also has this feature, and calculations also deliver on the low-energy shoulder ascribed as the Cr $1s \rightarrow L^{\bullet}(\alpha)$ transition, where the absorbing orbital is computed to comprise 35.5% Cr 3d, and most importantly, 1.4% Cr 4p character, which gives this peak intensity through the incorporation of dipole-allowed character.

The formulation of this electron transfer series is elegantly corroborated by the S K-edge spectra (Fig. 28). Overlooking the small amount of oxidized impurity (~15%), the spectrum of $[Cr^{III}(Cl_2\text{-bdt})_3]^{3-}$ ($S = 3/2$) has no prominent pre-edge features. The spectra of the monoanion and dianion have two pre-edge peaks: the first indicative of a dithiolene ligand radical at 2469.7 eV, where the intensity of this peak reflects the number of radicals with two in $[Cr^{III}(Cl_2\text{-bdt})(Cl_2\text{-bdt}^{\bullet})_2]^{1-}$ ($S = 1/2$) compared with one in $[Cr^{III}(Cl_2\text{-bdt})_2(Cl_2\text{-bdt}^{\bullet})]^{2-}$ ($S = 1$). Again the calculations augmented the experimental data to give a self-consistent picture for this tris(dithiolene)chromium electron transfer series (Fig. 29).

However, the missing member of the series, $[Cr(dithiolene)_3]^0$ ($S = 0$) has not been sufficiently characterized to unambiguously define its electronic structure, let alone its molecular structure. Only two molecules have ever been isolated, that being $[Cr(pdt)_3]^0$ by Schrauzer and Mayweg [69], and $[Cr(tfd)_3]^0$ by Holm and coworkers, where $(tfd)^{2-}$ is bis(trifluoromethyl)ethylenedithiolate [64]. Based on X-ray powder diffraction and electronic absorption spectroscopy [50], Gray et al. suggested that $[Cr(pdt)_3]^0$ is also trigonal prismatic given its similarity to $[V(pdt)_3]^0$ – known at the time to be trigonal prismatic – and $[V(pdt)_3]^{1-}$, which was recently shown to be more trigonal prismatic than the neutral compound [66]. DFT calculations predicted that a trigonal prismatic ($\Theta = 4.3^{\circ}$) neutral tris(dithiolene)chromium complex would comprise a Cr(IV) d^2 central ion encapsulated by a $(L_3)^{4-}$ tris(dithiolene) unit, i.e. two oxidized holes. The corresponding broken symmetry BS(3,3) calculation produced an octahedral structure ($\Theta = 49.7^{\circ}$) defined as Cr(III) d^3 ion bound by three monoanionic dithiolene radicals, $[Cr^{III}(L^{\bullet})_3]^0$, completely analogous to the dioxolene compound [58]. Although there is no crystal structure to confirm the complex geometry, calculations weigh heavily on the side of the octahedral structure, with this solution being 20 kcal mol^{-1} more stable.

5.3. Manganese and iron

The history of tris(dithiolene) chemistry of Mn and Fe is rather thin owing to the limited number of compounds synthesized. In 1968, McCleverty et al. described the preparation of $[Mn(mnt)_3]^{2-}$ ($S = 3/2$), $[Fe(mnt)_3]^{3-}$ ($S = 1/2$), and $[Fe(mnt)_3]^{2-}$ ($S = 1$) [61]. Prior to 2009, only the latter had been structurally characterized [79], and described as a low-spin Fe(IV) d^4 ion ($S = 1$) coordinated by three closed-shell dithiolate(2−) ligands. This assignment was supported by a change in the Mössbauer isomer shift of 0.14 mm s^{-1} [80]. What is so fascinating is the general idea that Fe(IV) will form so easily – aerial oxidation of solid $[Fe(mnt)_3]^{3-}$ on the bench gives the triplet dianionic $[Fe(mnt)_3]^{2-}$ complex. It turns out that there is "Fe(IV)" and then there is "Fe(IV)".

With only four isolated tris(dithiolene)manganese complexes [53,58,61,70,81], all of which are $S = 3/2$ dianions, the electronic structure is readily formulated as $[Mn^{IV}(dithiolato)_3]^{2-}$. The EPR spin Hamiltonian parameters reported for $[Mn^{IV}(mnt)_3]^{2-}$ and

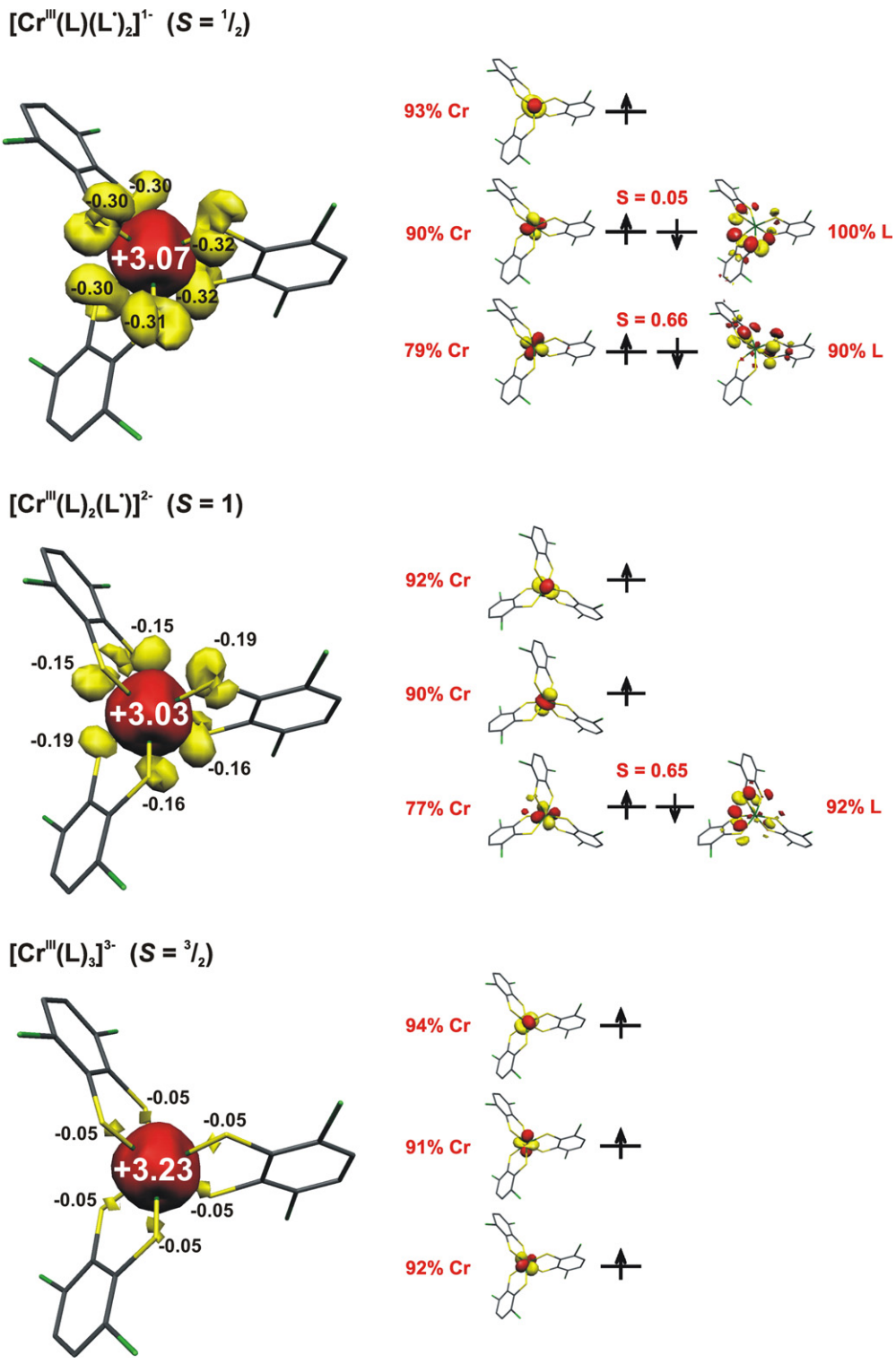

Fig. 29. Spin density plots of the $[Cr^{III}(Cl_2\text{-bdt})_3]^z$ ($z = 1-, 2-, 3-$) electron transfer series, as derived from B3LYP DFT calculations together with values of the spin density of the Mulliken analyses. Qualitative MO diagrams of the corresponding orbitals of magnetic pairs in $[Cr^{III}(Cl_2\text{-bdt})(Cl_2\text{-bdt}^{\bullet})_2]^{1-}$ and $[Cr^{III}(Cl_2\text{-bdt})_2(Cl_2\text{-bdt}^{\bullet})]^{2-}$ and quasi-restricted orbitals for $[Cr^{III}(Cl_2\text{-bdt})_3]^{3-}$ calculated at the B3LYP/TZVP level shown right [57].

$[Mn^{IV}(Cl_2\text{-bdt})_3]^{2-}$ are very much identical to $[Mn^{IV}(dtc)_3]^{1+}$, containing the redox inert diethyldithiocarbamate(1−) ligand [58]. Moreover, their S K-edge spectra are almost superimposable leaving no doubt that these are three dithiolate(2−) ligands. Not surprisingly, the Mn(IV) d^3 configuration leads to octahedral geometries as told by the crystallographically characterized $[Mn^{IV}(Cl_2\text{-bdt})_3]^{2-}$ ($\Theta = 48.2°$) [58], $[Mn^{IV}(mnt)_3]^{2-}$ ($\Theta = 49.9°$) [58] and $[Mn^{IV}(bdt)_3]^{2-}$ ($\Theta = 44.7°$) [81] dianions.

The Fe K-edge spectra of $[Fe(mnt)_3]^{3-}$ and $[Fe(mnt)_3]^{2-}$ are overlaid in Fig. 30 [57]. The shift of 0.8 eV in the rising-edge energy indicates an increase in Z_{eff} upon oxidation of the trianion. On the other hand, the pre-edge energy only shifts by 0.3 eV,

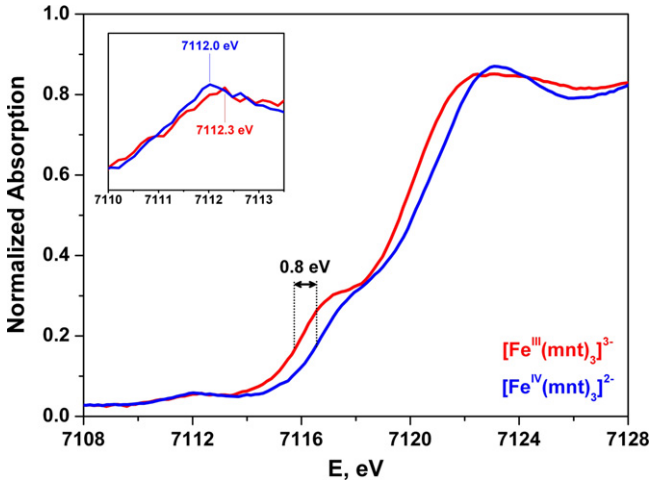

Fig. 30. Overlay of the Fe K-edge XAS spectra of $[Fe(mnt)_3]^{2-/3-}$. The inset shows an expansion of the pre-edge region [57].

though in the opposite direction. The expected ~1 eV shift is counteracted by a decrease in the trigonal twist angle ($\Theta = 53.4^\circ$ for $[Fe(mnt)_3]^{3-}$; $\Theta = 46.6^\circ$ $[Fe(mnt)_3]^{2-}$) which lowers the pre-edge transition energy for the dianion.

The deconvoluted S K-edge spectra compared in Fig. 31 each shows three pre-edge peaks (red, blue, and green). Using information gained from the S K-edge assignment of Na_2mnt and $[Fe^{III}(cyclam)(mnt)]^{1+}$ [28], these three peaks were assigned as transitions to the half-filled t_{2g} orbital(s), empty Fe–S antibonding e_g orbitals, and the C–S π^* MO of the mnt ligands (Table 3)

The salient feature of this comparison is the significant increase in the intensity of the S $1s \rightarrow t_{2g}$ peak in $[Fe^{IV}(mnt)_3]^{2-}$, and its shift to lower energy due to the larger Z_{eff} of a +IV ion rather than the generation of a ligand hole. This is elegantly demonstrated in Fig. 32 which shows an overlay of the S K-edge spectra of $[M(mnt)_3]^{2-}$ (M = V, Cr, Mn, Fe) [57,58,66]. Only the chromium complex has a genuine ligand radical pre-edge peak at 2469.9 eV and is thus formulated as $[Cr^{III}(mnt)_2(mnt^{\bullet})]^{2-}$ [58]. The remaining complexes have three $(mnt)^{2-}$ ligands coordinating a +IV central ion [57,58,66]. Moving left to right across the first row transition metals, the energy of this S $1s \rightarrow t_{2g}$ transition becomes lower in energy due to the increasing Z_{eff} of the metal ion.

It is with DFT calculations that the true nature of the Fe(IV) ion is expressed. The case for $[Fe^{III}(mnt)_3]^{3-}$ ($S = 1/2$) is straightforward; the Mulliken spin density plot in Fig. 33 (left) sees one unpaired electron in an Fe t_{2g} orbital. The Mössbauer parameters – aside from the sign of the quadrupole splitting – are in excellent agreement with the experimental data (Table 4). In silico one-electron oxidation to the dianion afforded two possibilities: (1) a simple spin-unrestricted $S = 1$ approach, or (2) a broken symmetry BS(3,1) which encompasses an intermediate-spin ferric ion ($S_{Fe} = 3/2$) coordinated by one $(mnt^{\bullet})^{1-}$ ligand radical ($S_L = 1/2$). In the latter approach, the solution converged back to the simple spin-unrestricted triplet ground state, i.e. no ligand radicals were found

Table 3
Energies (eV) of the pre-edge transitions and the dipole-allowed edge feature [57].

	$E(t_{2g})$	$E(e_g)$	$E(L_{\pi^*})$	E(rising-edge)
$[Fe^{III}(mnt)_3]^{3-}$	2470.5	2470.9	2471.5	2472.9
$[Fe^{IV}(mnt)_3]^{2-}$	2470.3	2470.6	2471.8	2473.3
Na_2mnt[a]	–	–	2471.1	2472.3
$[Fe^{III}(cyclam)(mnt)]^{2+}$	2470.2	2470.9	2471.9	2473.3

[a] From Ref. [32].

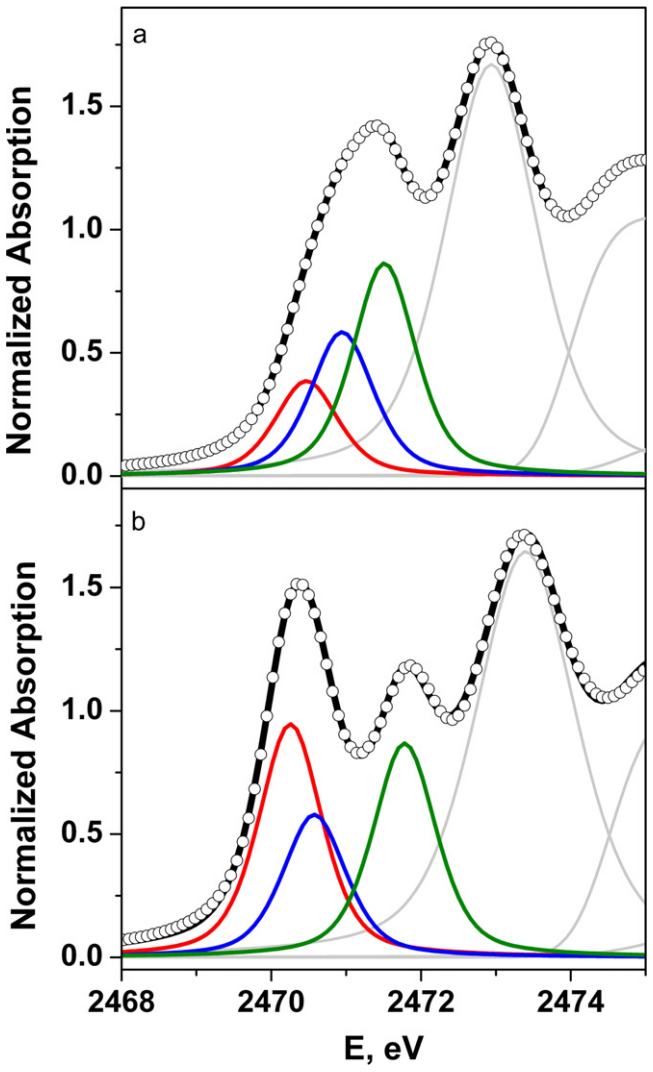

Fig. 31. Pseudo-Voigt deconvoluted S K-edge spectra of (a) $[Fe^{III}(mnt)_3]^{3-}$, and (b) $[Fe^{IV}(mnt)_3]^{2-}$. The red peak indicates the S $1s \rightarrow t_{2g}$ transition; the blue peak the S $1s \rightarrow e_g$ transition; the green peak the S $1s \rightarrow L_{\pi^*}$ transition [57].

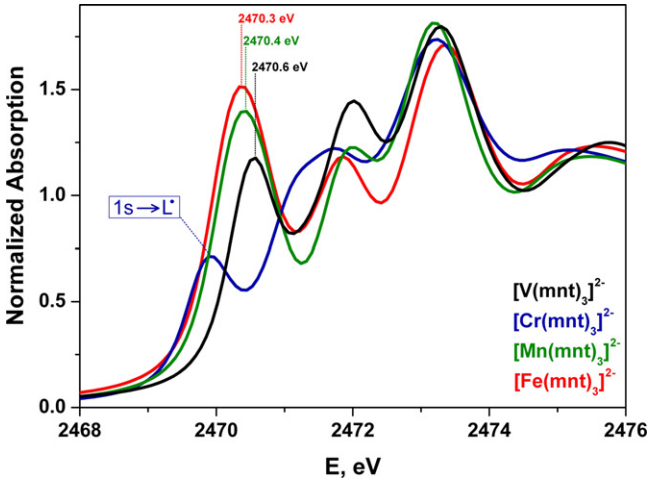

Fig. 32. Overlay of the normalized S K-edge XAS spectra of $[M(mnt)_3]^{2-}$ (M = V, Cr, Mn, Fe) [57,58,66].

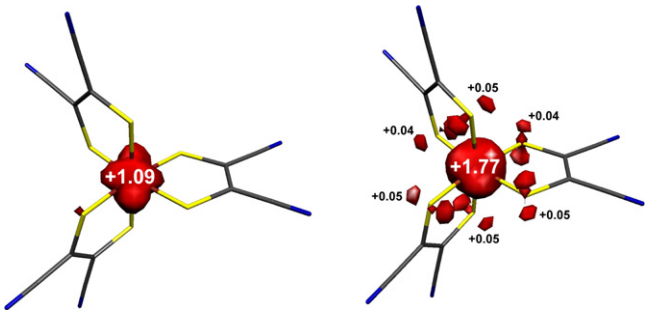

Fig. 33. Mulliken spin density plots for $[Fe^{III}(mnt)_3]^{3-}$ (left) and $[Fe^{IV}(mnt)_3]^{2-}$ (right) obtained from B3LYP/TZVP DFT calculations [57].

computationally. The calculated Mössbauer parameters are once again mirrored the experimental result (Table 4).

The nature of this Fe(IV) species is best visualized in the Mulliken spin density plot (Fig. 33, right), where +1.77 spins are found on Fe, +0.27 on the sulfur atoms, and −0.03 on the olefinic carbon atoms. This underscores a highly covalent system for this $Fe^{IV}S_6$ polyhedron, and starkly contrasts the case for $[(N_4)Fe(dithiolene)]^{2+}$, where replacing two S,S′-coordinated dithiolate(2−) ligands for a tetradentate N_4 cyclam reduces the covalency and pushes the electronic structure to a $[Fe^{III}(cyclam)(mnt^{\bullet})]^{2+}$ singlet diradical rather than stabilization of an Fe(IV) [28].

5.4. Molybdenum and tungsten

Unlike the late transition metal square planar bis(dithiolene) complexes where a common electronic structure prevails for most metals, the early transition metal tris(dithiolene) compounds show profound differences across the period and down groups. A case in point is group 6: Cr, Mo, and W. As described above, experimental and theoretical data for the neutral tris(dithiolene)chromium complex point toward an octahedral compound formulated as $[Cr^{III}(L^{\bullet})_3]^0$ akin to its tris(dioxolene) analogue [58,59]. Moving down the group to the second row, neutral tris(dithiolene)molybdenum complexes, which are abundant in the literature [43], have for their entire existence been cast as $[Mo^{VI}(L)_3]^0$. A similar position has been described for tungsten, in that the metal in its highest oxidation state (+VI) is coordinated by three dithiolate(2−) ligands. It was not until 2007 that this position was revised [78], and it was the combination of IR and XAS that motivated the reformulation. Two compounds from the three-membered electron transfer series, namely $[Mo(tbbdt)_3]^z$ ($z = 0$, 1−) were isolated, structurally characterized, and their IR spectra recorded. The monoanionic compound shows no ν(C=S•) stretch, whereas the neutral complex does, at 1106 cm^{-1}. The tungsten analogue exhibited an identical stretch, and implied these neutral compounds could not be described as Mo(VI) and W(VI) species.

Sulfur K-edge XAS provided the final nail in the coffin of a M(VI) d^0 ion in these neutral species. The S K-edge spectrum of $[Mo^{V}(tbbdt)_3]^{1-}$ displays a single intense pre-edge peak at 2470.8 eV typical for S,S′-coordinated closed-shell dithiolate ligands (Fig. 34). On the other hand, the S K-edge spectra of $[Mo(tbbdt)_3]^0$ and $[W(tbbdt)_3]^0$ exhibited two pre-edge peaks at

Table 4
Comparison of the calculated and experimental (in parentheses) Mössbauer parameters [57].

	δ (mm s^{-1})	ΔE_Q (mm s^{-1})	η^a
$[Fe^{III}(mnt)_3]^{3-}$	0.37 (0.36)	+1.90 (−1.68)	0.98 (0.85)
$[Fe^{IV}(mnt)_3]^{2-}$	0.38 (0.39)	−2.35 (−1.77)	0.65 (0.62)

[a] Asymmetry parameter of the electric field gradient.

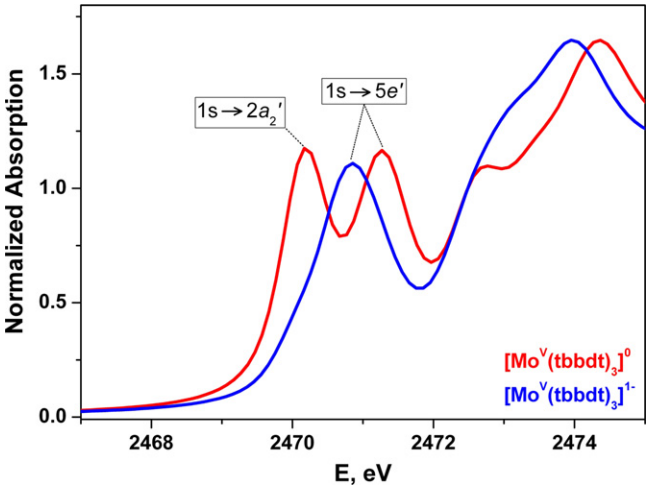

Fig. 34. Overlay of the normalized S K-edge XAS spectra of $[Mo(tbbdt)_3]^{0/1-}$ [78].

~2470.2 eV and 2471.3 eV. The lower energy feature was assigned as a S 1s → L• transition – the radical fingerprint – whereas the second pre-edge feature corresponds to a S 1s → 5e′ transition, as seen in the spectrum of the monoanion and moved to higher energy owing to an oxidized tris(dithiolene) ligand set. The electron transfer series was therefore defined as given in Scheme 9 where the neutral compound is a singlet diradical owing to the strongly antiferromagnetic coupling of the ligand radical with the Mo(V) d^1 center [78].

This interpretation was modified by Solomon and co-workers [82] in a meaty spectroscopic and theoretical tome deploying S K-edge XAS on a series generated by Holm et al. $[Mo(mdt)3]^z$ ($z = 0$, 1−, 2−) [83,84]. The S K-edge spectra for the three-membered electron transfer series are overlaid in Fig. 35, and were interpreted as all containing a low-spin Mo(IV) d^2 central ion with a successive oxidation of the tris(dithiolene) ligand set from $(L_3)^{6-}$ in the dianion, to $(L_3)^{5-\bullet}$ in the monoanion, to $(L_3)^{4-}$ – two valence holes – in the neutral (Scheme 10).

There is clearly a different spectral profile for the monoanionic $[Mo(mdt)_3]^{1-}$ compared with our spectrum of $[Mo^{V}(tbbdt)_3]^{1-}$; the spectra of these two complexes are contrasted in Fig. 36. The former, containing an "olefinic" dithiolene ligand (^{B}L) exhibits two pre-edge peaks with the first being the hallmark of a dithiolene radical, while the second is the previously noted S 1s → 5e′ transi-

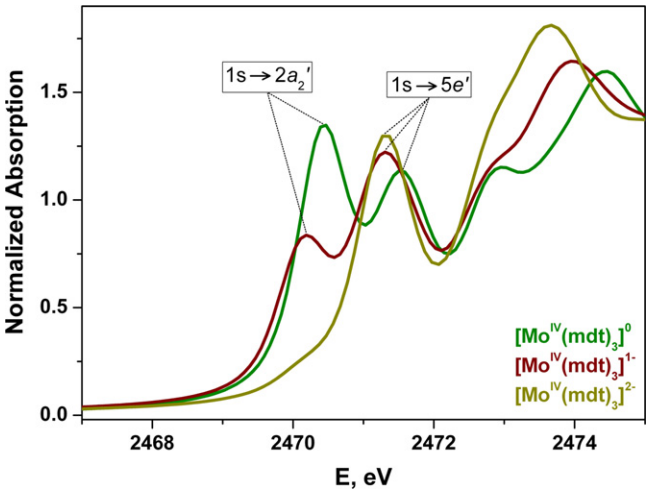

Fig. 35. Comparison of the normalized S K-edge XAS spectra of $[Mo(mdt)_3]^z$ ($z = 0$, 1−, 2−) [82].

$$[Mo^{V}(^{A}L_3^{5-\bullet})]^0 \underset{-e}{\overset{+e}{\rightleftharpoons}} [Mo^{V}(^{A}L_3^{6-})]^{1-} \underset{-e}{\overset{+e}{\rightleftharpoons}} [Mo^{IV}(^{A}L_3^{6-})]^{2-}$$
$$(S=0) \qquad (S={}^1/_2) \qquad (S=0)$$

Scheme 9. Three-membered electron transfer series for $[Mo(^{A}L_3)]^0$, where $(^{A}L_3)^{6-}$ represents a tris(aromatic-1,2-dithiolato) ligand set [78].

$$[Mo^{IV}(^{B}L_3^{4-})]^0 \underset{-e}{\overset{+e}{\rightleftharpoons}} [Mo^{IV}(^{B}L_3^{5-\bullet})]^{1-} \underset{-e}{\overset{+e}{\rightleftharpoons}} [Mo^{IV}(^{B}L_3^{6-})]^{2-}$$
$$(S=0) \qquad (S={}^1/_2) \qquad (S=0)$$

Scheme 10. Three-membered electron transfer series for $[Mo(^{B}L_3)]^0$, where $(^{B}L_3)^{6-}$ represents a olefinic tris(dithiolene) ligand set.

tion. The complex is formulated as $[Mo^{IV}(L_3^{5-\bullet})]^{1-}$, and contrasts the aromatic-1,2-dithiolate(^{A}L) analogue, that is $[Mo^{V}(tbbdt)_3]^{1-}$, with three dithiolate(2−) ligands.

These electronic structural differences are a consequence of the complex geometries. The distorted octahedral $[Mo^{V}(tbbdt)_3]^{1-}$ ($\Theta = 31.9°$) [78] facilitates a configurational interaction between the $3a_1'$ (Mo $4d_{z^2}$ orbital) and $3a_1''$ MOs (both transform as a_1 in the D_3 symmetry of a distorted octahedron) that destabilizes the d_{z^2} orbital relative to the purely ligand-based $2a_2'$ MO. The trigonal twist is absent in $[Mo^{IV}(mdt)_3]^{1-}$ ($\Theta = 1.6°$) [84], thus the $2a_2'$ is singly occupied.

Solomon et al. applied their standard method to quantify the covalency for the $[Mo(mdt)_3]^z$ ($z = 0, 1-, 2-$) series [32,33], where the covalency (or S 3p character), α^2, is directly proportional to the peak intensity, D_0 described by Eq. (1) in Section 4.1. The calculated and experimental covalencies (S 3p content) were in very good agreement across the series. Additionally, the consequence of the chelate fold (Fig. 21) that represents a lowering of symmetry to C_{3h} in the neutral complex reversed the computational observations of Campbell and Harris [85]. The S 3p content of the $2a_2'$ MO decreases due to a configurational interaction between the filled $3a_1'$ HOMO and $2a_2'$ LUMO (both transform as a' in C_{3h} symmetry) upon dithiolene folding leads to stabilization of the Mo d_{z^2} orbital and concomitant destabilization of the $2a_2'$ MO leading to a greater stabilization of the C_{3h} distorted complex over a purely trigonal prismatic D_{3h} one (Fig. 21). Campbell and Harris deemed the opposite occurred affording a Mo(VI) d^0 ion and fully occupied ligand π-donor orbitals [85].

The overlay of the S K-edge spectra of $[Mo(tbbdt)_3]^0$ and $[Mo(mdt)_3]^0$ shown in Fig. 37 present a rather interesting comparison, since the former was classified as Mo(V) d^1 with one valence hole; the latter low-spin Mo(IV) d^2 with two valence holes. There is no disputing the keen similarity between the two spectra, such that Solomon and co-workers declared that $[Mo(tbbdt)_3]^0$ has 1.4 valence holes as derived from the first pre-edge peak intensity, calibrated by the spectrum of $[Mo^{IV}(mdt)_3]^{1-}$ (1 hole = 0.6 units of intensity). DFT calculations declared that a D_3 distortion (trigonal twist, Fig. 38), which leads to a Mo(V) d^1 and $(L_3)^{5-\bullet}$ configuration, was not as energetically favorable as a $D_{3h} \rightarrow C_{3h}$ distortion (dithiolene folding) that maintains the trigonal prismatic MoS_6 core and stabilizes the d_{z^2} orbital relative to the $2a_2'$ orbital. Thus, it was con-

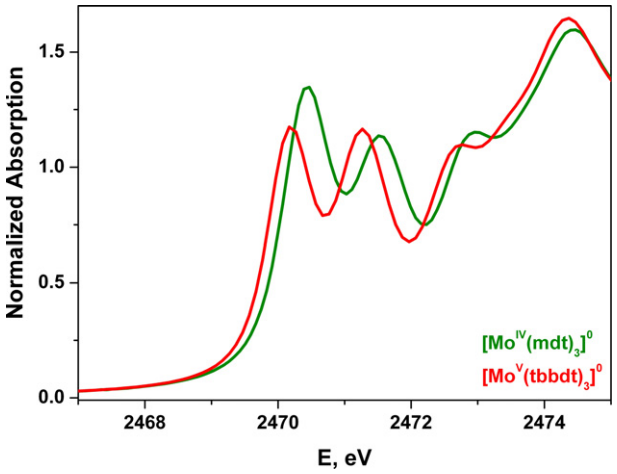

Fig. 37. Comparison of the normalized S K-edge XAS spectra of $[Mo^{IV}(mdt)_3]^0$ and $[Mo^{V}(tbbdt)_3]^0$ [82].

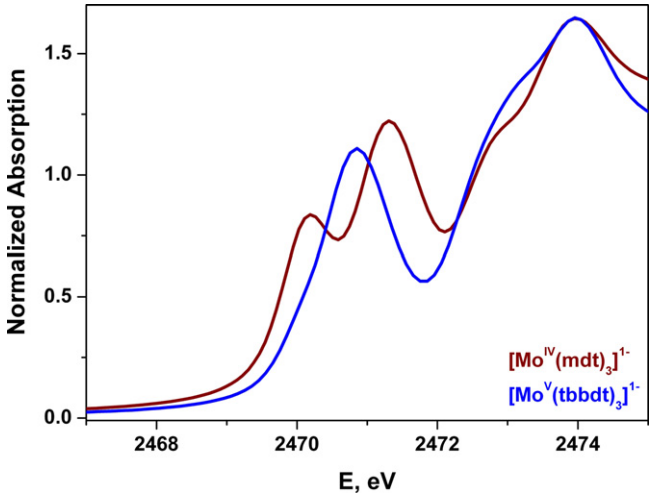

Fig. 36. Comparison of the normalized S K-edge XAS spectra of $[Mo^{IV}(mdt)_3]^{1-}$ and $[Mo^{V}(tbbdt)_3]^{1-}$ [82].

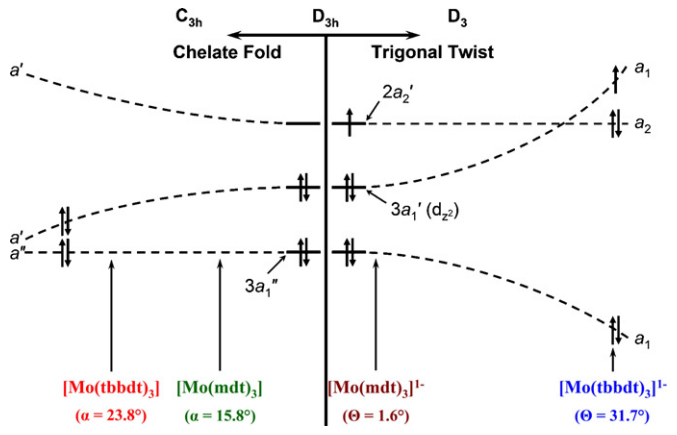

Fig. 38. Diagram showing the orbital interactions with chelate fold (left) and trigonal (Bailar) twist (right) distortions for formally d^0 and d^1 tris(dithiolene) complexes, respectively. The approximate values of the major distortion in the neutral (left) and monoanionic (right) complexes are also indicated [82].

cluded, as detailed in Fig. 38, that both neutral complexes are best viewed as $[Mo^{IV}(L_3^{4-})]^0$.

This is by no means the end of the discussion, for instance, neither group ever sought to publish the Mo K-edge spectra for their respective series. For $[Mo(tbbdt)_3]^{0/1-}$, according to our description of both having a physical Mo(V) oxidation state, they should have overlapping rising-edge energies barring any influence of the noted difference in their trigonal twist angles. Likewise for the $[Mo^{IV}(mdt)_3]^{0/1-/2-}$ series. Secondly, it is worth comparing the S K-pre-edge intensities for two sets of isoelectronic complexes: $[Mo^{IV}(pdt)_3]^0$ and $[Re^{V}(pdt)_3]^{1+}$, and $[Mo^{IV}(pdt)_3]^{1-}$ and $[Re^{V}(pdt)_3]^0$ (Fig. 39) [86], given that the electronic structure of the tris(dithiolene)rhenium series has been unambiguously defined (*vide infra*).

The former are both described as d^2 central ions encapsulated by a $(L_3)^{4-}$ ligand set; the latter with a one-electron reduced ligand set $(L_3)^{5-\bullet}$. Even keeping in mind that $[Re^{V}(pdt)_3]^{1+}$ optimizes as D_{3h} with no hint of chelate folding [87], there is a glaringly obvious lack of intensity for the first pre-edge peak in the molybdenum series compared with the rhenium series for what are transitions to the empty ligand-centered $2a_2'$ orbital. Certainly, the S 3p content will change owing to the different covalencies inherent to Mo–S and Re–S bonds. However, the data already published on these systems maintains the calculated S 3p content of the $2a_2'$ orbital lies in the range of 60–70%, not enough to account for the vast disparity in the intensity of the first pre-edge peak presented in Fig. 39. One of the salient points that came out of the DFT analysis of the bis(dithiolene) series were the different values for the dipole integral $I(S)$ for transitions to σ^* and π^* acceptor orbitals [31]. For tris(dithiolenes), the first pre-edge is a transition to an essentially nonbonding ligand-based orbital, ignoring for the moment the degree of its nonbonding nature that is modulated by configurational mixing brought about by chelate folding. Perhaps a different $I(S)$ value is warranted, however, unlike the routine consistency seen across the square planar bis(dithiolene) series with so many metals, the same depth is not yet available in tris(dithiolene) compounds for such a determination.

5.5. Rhenium

An X-ray structural study of $[Re(pdt)_3]^0$ ($S = 1/2$) in the early 1960s led to the discovery of the first six-coordinate compound with a trigonal prismatic structure [48]. This was soon followed by $[Mo(edt)_3]^0$ ($S = 0$) [49], and $[V(pdt)_3]^0$ ($S = 1/2$) [50,51] – a periodic trifecta – such that it was quickly realized that this unique geometry was synonymous amongst neutral tris(dithiolene) complexes of early transition metals. Recognizing an intrinsic electronic effect was operative, the pioneers of dithiolene chemistry sought

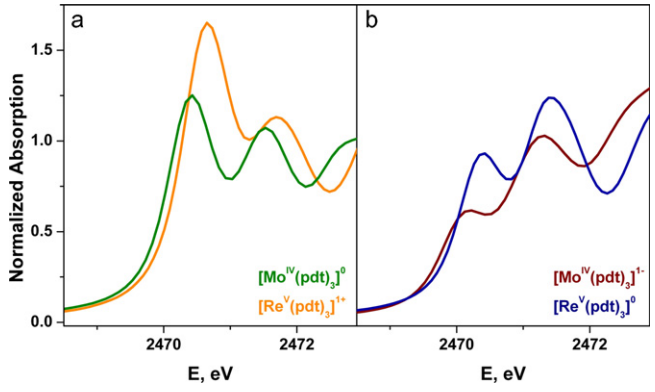

Fig. 39. Comparison of the normalized S K-edge spectra of isoelectronic (a) $[Mo^{IV}(pdt)_3]^0$ and $[Re^{V}(pdt)_3]^{1+}$, and (b) $[Mo^{IV}(pdt)_3]^{1-}$ and $[Re^{V}(pdt)_3]^0$ [86].

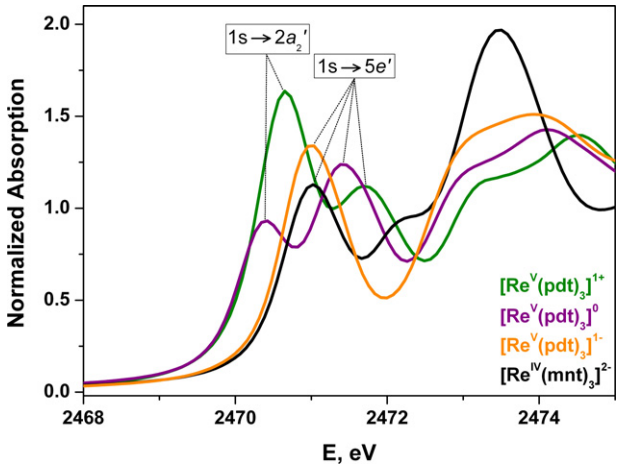

Fig. 40. Overlay of the normalized S K-edge XAS spectra of $[Re^{V}(pdt)_3]^z$ ($z = 1+, 0, 1-$) and $[Re^{IV}(mnt)_3]^{2-}$ [86].

answers from molecular orbital calculations. As mentioned previously, the calculated electronic configuration for $[V^{IV}(pdt)_3]^0$ of $(4e')^2(3a_1')^1(2a_2')^0(5e')^0$ was absolutely correct as successive generations would discover with new spectroscopic forays into this field [51,66]. However, neutral tris(dithiolene)rhenium was more challenging, as can be gleaned from the dearth of literature on this subject post the 1966 trigonal prismatic revolution (which of course makes it so easy to review). As a third row transition metal, there was simply no basis set to describe the Re atom; there was not an abacus on the planet that could handle that many electrons and the relativistic effects. Not deterred by this Gray et al. [88] proposed a Re(VI) d^1 central ion implying three dithiolate(2−) ligands: $[Re^{VI}(L_3^{6-})]^0$ [89]. The Schrauzer and Mayweg approach utilized a different coulombic potential (i.e. zero line) that generated a different ordering of the frontier orbitals that, in this day and age, led to a $[Re^{IV}(L_3^{4-})]^0$ formulation [69]. Al-Mowali and Porte recognized these electronic structures were incongruous with the EPR spectrum, and put forth a $[Re^{V}(L_3^{5-\bullet})]^0$ formulation – a ligand-centered paramagnet [90]. It turns out they were correct, though their analysis of the frozen solution EPR spectrum was erroneous. As it happens, this spectrum is the most amazing continuous wave EPR spectrum ever seen and attributable to the intrinsic properties of a Re(V) d^2 ion in a trigonal prismatic ligand field [87]; the spectrum alone proves the formulation of Al-Mowali and Porte to be correct.

This renders $[Re^{V}(L_3^{5-\bullet})]^0$ as a reference for the rest of the $[Re(dithiolene)_3]^z$ ($z = 1+, 0, 1-, 2-$) series; the neutral compound can be reversibly one-electron oxidized, and twice one-electron reduced [70,87,88]. The frozen solution EPR spectrum of the dianion unambiguously indicated a $[Re^{IV}(L_3^{6-})]^{2-}$ electronic structure with highly anisotropic g values and large magnetic hyperfine interaction due to the $^{185,187}Re$ ($I = 5/2$, 100% natural abundance) isotopes [87]. As in the case of the vanadium series, the diamagnetic members have been overlooked.

A simple S K-edge XAS study conveniently cleared up any mystery surrounding this electron transfer series. The S K-edge spectra for $[Re^{V}(pdt)_3]^z$ ($z = 1+, 0, 1-$) and $[Re^{IV}(mnt)_3]^{2-}$ are overlaid in Fig. 40 [86]. The spectrum of the neutral, whose electronic structure is set in stone, shows two pre-edge peaks defined as S 1s → $2a_2'$ (ligand hole) and S 1s → $5e'$ transitions that have S 3p character through covalent bonds with the Re $5d_{x^2-y^2,xy}$ orbitals. From a purely qualitative view, oxidation to the monocation sees the first pre-edge peak double in intensity revealing a ligand-centered oxidation to a $[Re^{V}(L_3^{4-})]^{1+}$ ($S = 0$) species. One-electron reduction of the neutral compound fills the $2a_2'$ MO such that the spectrum of

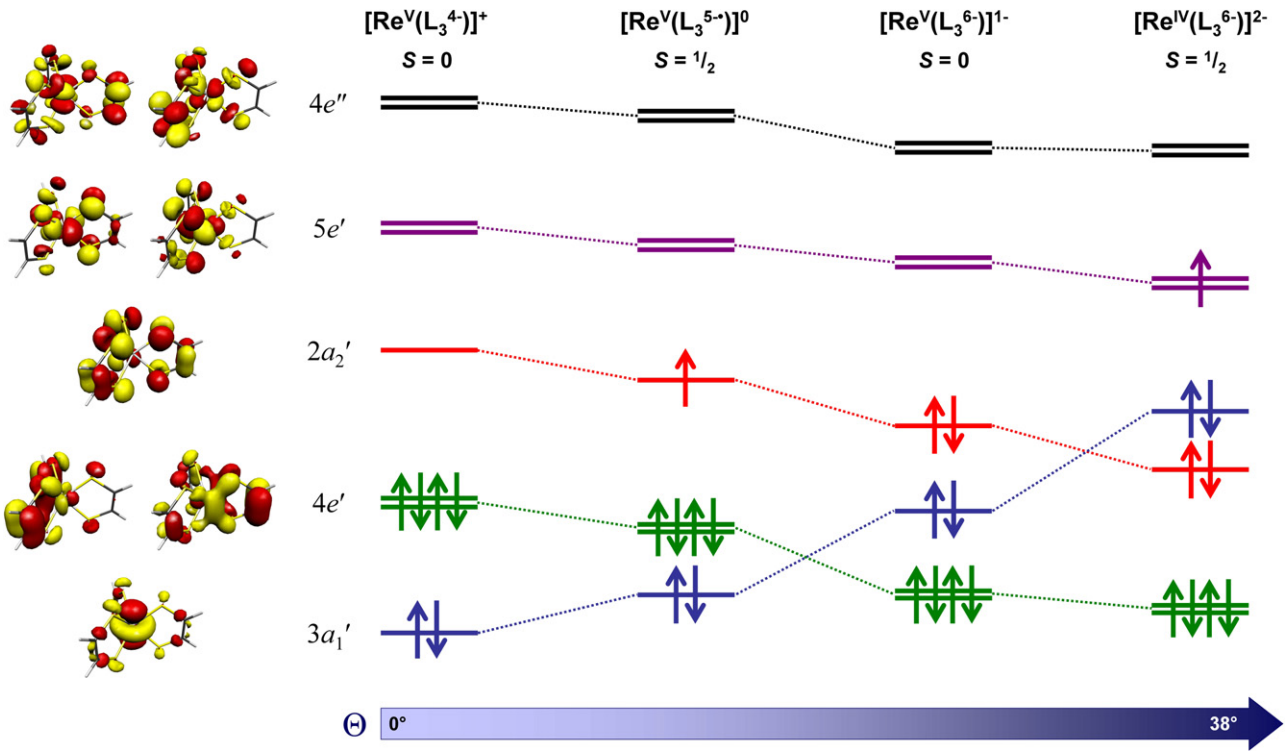

Fig. 41. Qualitative MO scheme depicting the ordering of the frontier orbitals for the $[Re(L_3)]^z$ ($z = 1+, 0, 1-, 2-$) electron transfer series derived from B3LYP/ZORA DFT calculations. The MOs shown left are derived from the $[Re(edt)_3]^{1+}$ calculation with D_{3h} symmetry labels. The arrow represents a twist away from trigonal prismatic geometry for the monocation and neutral species, to a distorted trigonal prism for the monoanionic complexes, and finally a distorted octahedral dianionic species [87].

the monoanion has only one pre-edge peak attributed to a $1s \rightarrow 5e'$ transition that is at slightly lower energy than the corresponding peak in $[Re^V(pdt)_3]^{1+}$ and $[Re^V(pdt)_3]^0$ because the sulfur has been reduced. Finally, this pre-edge peak in $[Re^{IV}(mnt)_3]^{2-}$ ($S = 1/2$) has diminished intensity since one of the four holes in the $5e'$ level is now occupied. The calculated spectra mirror the experimental data almost perfectly [87].

The electronic structures of this series are visualized in the qualitative MO scheme provided in Fig. 41. Like with tris(dithiolene)vanadium, the first three members differ in the occupation of the $2a_2'$ MO – ligand-centered redox events – after which the $5e'$ level begins to fill. The occupancy of these orbitals leads to a twisting of the geometry away from trigonal prismatic (calculated for the monocation; experimentally measured for the neutral) to distorted trigonal for the monoanion, and finally to a distorted octahedral polyhedron for the dianionic species – $[Re^{IV}(mnt)_3]^{2-}$ has a crystallographic trigonal twist of 38.3° [91].

6. Conclusion

The spectroscopic veil of silence that shrouded sulfur has been lifted by the application of sulfur K-edge XAS. The technique allows the sulfur atoms of any given transition metal dithiolene complex to be directly probed, a possibility previously limited to costly ^{33}S-labeled EPR experiments of paramagnetic compounds. The outcome of these S K-edge XAS studies was a direct experimental measure of the noninnocence of dithiolene ligands, particularly in the case of bis(dithiolene) systems, wherein quantification of the redox-active orbital revealed greater than 50% sulfur 3p character. This evokes an "inverted bond" scenario, and the members of any bis(dithiolene) and tris(dithiolene) electron transfer series that are interrelated by one-electron redox steps see electrons removed/added from the redox-active $2b_{2g}$ or $2a_2'$ orbitals that are a predominantly ligand in character. This is the very essence of a redox noninnocent ligand, and underscores the original premise that the chelating dithiolene was probably the first well recognized member of the ever growing list of noninnocent bidentate ligands.

It is quite amazing (and generally annoying for the rest of us!) that the early pioneers of transition metal dithiolene chemistry could intuitively recognize the redox noninnocence of these ligands at the very genesis of transition metal dithiolene chemistry despite the dearth of spectroscopic evidence to support their assignments. It was the very notion that a dithiolate ligand in a coordination compound could be one-electron oxidized to a radical monoanion, and potentially further to a neutral dithioketone, that prompted McCleverty to coin the term "dithiolene" [92]. The purpose was to have one encompassing term for all forms of the ligand without giving bias to one particular structure or valence formalism [93]. And it worked, for now we can use the word dithiolene and obviate the need to specify the ligand oxidation level. The consequence of streamlining the nomenclature was that the dithiolene radical was more or less lost from our chemistry vernacular, and it was the prudent use of sulfur K-edge XAS that brought it back into consideration when defining the electronic structures of these intriguing coordination compounds.

Acknowledgments

We are grateful for financial support from the Fonds der Chemischen Industrie. S.S. thanks the Max-Planck-Society for a postdoctoral fellowship. SSRL operations are funded by the Department of Energy, Office of Basic Energy Sciences. The Structural Molecular Biology program is supported by the National Institutes of Health, National Center for Research Resources, Biomedical Technology Program and by the Department of Energy, Office of Biological Environmental Research.

References

[1] E.I. Stiefel, J.H. Waters, E. Billig, H.B. Gray, J. Am. Chem. Soc. 87 (1965) 3016.
[2] Our definition for a formal oxidation number (state) of a given metal ion in a coordiation compound is a nonmeasurable integer which is commonly defined as the charge left on the metal after all ligands have been removed in their normal, closed-shell configuration (L.S. Hegedus in Transition Metals in the Synthesis of Complex Organic Molecules, University Science Books: Mill Valley, CA, 1994, p. 3). Alas, the monoanionic and neutral bis(dithiolene)nickel complexes are formally Ni(III) and Ni(IV), respectively, however, they have physical oxidation states of neither Ni(III) nor Ni(IV)—the salient point of this publication. A physical or spectroscopic oxidation number (state) is one derived from a known d^n configuration of a metal ion in a coordination compound. (C. K. Jørgensen in Oxidation Numbers and Oxidation States, Springer: Heidelberg, Germany, 1969).
[3] H.B. Gray, E. Billig, J. Am. Chem. Soc. 85 (1963) 2019.
[4] A.H. Maki, N. Edelstein, A. Davison, R.H. Holm, J. Am. Chem. Soc. 86 (1964) 4580.
[5] G.N. Schrauzer, V.P. Mayweg, J. Am. Chem. Soc. 87 (1965) 3585.
[6] H.B. Gray, R. Williams, I. Bernal, E. Billig, J. Am. Chem. Soc. 84 (1962) 3596.
[7] S.I. Shupack, E. Billig, R.J.H. Clark, R. Williams, H.B. Gray, J. Am. Chem. Soc. 86 (1964) 4594.
[8] R. Eisenberg, J.A. Ibers, R.J.H. Clark, H.B. Gray, J. Am. Chem. Soc. 86 (1964) 113.
[9] G.N. Schrauzer, V. Mayweg, J. Am. Chem. Soc. 84 (1962) 3221.
[10] G.N. Schrauzer, V.P. Mayweg, J. Am. Chem. Soc. 87 (1965) 1483.
[11] A. Davison, N. Edelstein, R.H. Holm, A.H. Maki, Inorg. Chem. 2 (1963) 1227.
[12] A. Davison, N. Edelstein, R.H. Holm, A.H. Maki, J. Am. Chem. Soc. 85 (1963) 2029.
[13] G.N. Schrauzer, H.N. Rabinowitz, J. Am. Chem. Soc. 90 (1968) 4297.
[14] R.D. Schmitt, A.H. Maki, J. Am. Chem. Soc. 90 (1968) 2288.
[15] R.H. Holm, A.L. Balch, A. Davison, A.H. Maki, T.E. Berry, J. Am. Chem. Soc. 89 (1967) 2866.
[16] B.S. Lim, D. Fomitchev, R.H. Holm, Inorg. Chem. 40 (2001) 4257.
[17] K. Ray, T. Weyhermüller, F. Neese, K. Wieghardt, Inorg. Chem. 44 (2005) 5345.
[18] D. Herebian, K. Wieghardt, F. Neese, J. Am. Chem. Soc. 125 (2005) 10997.
[19] V. Bachler, O. Gottfried, F. Neese, K. Wieghardt, Inorg. Chem. 41 (2002) 4179.
[20] B. Hedman, P. Frank, S.F. Gheller, A.L. Roe, W.E. Newton, K.O. Hodgson, J. Am. Chem. Soc. 110 (1988) 3798.
[21] (a) T. Glaser, B. Hedman, K.O. Hodgson, E.I. Solomon, Acc. Chem. Res. 33 (2000) 859;
(b) E.I. Solomon, B. Hedman, K.O. Hodgson, A. Dey, R.K. Szilagyi, Coord. Chem. Rev. 249 (2005) 97.
[22] B. Hedman, K.O. Hodgson, E.I. Solomon, J. Am. Chem. Soc. 112 (1990) 1643.
[23] C. Milsmann, E. Bothe, E. Bill, T. Weyhermüller, K. Wieghardt, Inorg. Chem. 48 (2009) 6211.
[24] (a) C.G. Pierpont, Coord. Chem. Rev. 216–217 (2001) 99;
(b) C.G. Pierpont, Coord. Chem. Rev. 219–221 (2001) 415;
(c) C.G. Pierpont, C.W. Lange, Prog. Inorg. Chem. 41 (1994) 331.
[25] C.G. Pierpont, R.M. Buchanan, Coord. Chem. Rev. 38 (1981) 45.
[26] P.A. Wicklund, L.S. Beckmann, D.G. Brown, Inorg. Chem. 15 (1976) 1996.
[27] R.D. Webster, G.A. Heath, A.M. Bond, J. Chem. Soc. Dalton Trans. (2001) 3189.
[28] C. Milsmann, G.K. Patra, E. Bill, T. Weyhermüller, S. DeBeer George, K. Wieghardt, Inorg. Chem. 48 (2009) 7430.
[29] C. Remenyi, M. Kaupp, J. Am. Chem. Soc. 127 (2005) 11399.
[30] C. Milsmann, E. Bill, T. Weyhermüller, S. DeBeer George, K. Wieghardt, Inorg. Chem. 48 (2009) 9754.
[31] K. Ray, S. DeBeer George, E.I. Solomon, K. Wieghardt, F. Neese, Chem. Eur. J. 13 (2007) 2783.
[32] R. Sarangi, S. DeBeer George, D. Jackson Rudd, R.K. Szilagyi, X. Ribas, C. Rovira, M. Almeida, K.O. Hodgson, B. Hedman, E.I. Solomon, J. Am. Chem. Soc. 129 (2007) 2316.
[33] R.K. Szilagyi, B.S. Lim, T. Glaser, R.H. Holm, B. Hedman, K.O. Hodgson, E.I. Solomon, J. Am. Chem. Soc. 125 (2003) 9158.
[34] K. Ray, T. Petrenko, K. Wieghardt, F. Neese, Dalton Trans. (2007) 1552.
[35] J.E. Huyett, S.B. Choudhury, D.M. Eichhorn, P.A. Bryngelson, M.J. Maroney, B.M. Hoffman, Inorg. Chem. 37 (1998) 1361.
[36] F. Neese, B. Hedman, K.O. Hodgson, E.I. Solomon, Inorg. Chem. 38 (1999) 4854.
[37] K. Rose, S.E. Shadle, T. Glaser, S. de Vries, A. Cherepanov, G.W. Canters, B. Hedman, K.O. Hodgson, E.I. Solomon, J. Am. Chem. Soc. 121 (1999) 2353.
[38] S.E. Shadle, J.E. Penner-Hahn, H.J. Schugar, B. Hedman, K.O. Hodgson, E.I. Solomon, J. Am. Chem. Soc. 115 (1993) 767.
[39] It is most important to note, that our use of the "L•" notation to represent a ligand radical is not meant to imply that the radical or hole is localized on one ligand. It is apparent from experimental and theoretical examination that the redox-active $2b_{2g}$ MO involves equal contribution from both ligands, and that the unpaired electron is delocalized. Therefore, these S = 1/2 complexes are described as Class III mixed valence ligand radicals, however we continue to use the "L•" notation because it simplifies both electron counting and compound formulation. The extent of spin polarization, i.e. singlet diradical character, in neutral bis(dithiolenes) of Ni, Pd, Pt, and the monocationic bis(dithiolene) complex of gold is still very much a matter of debate. The available experimental data does give credence to such a formulation, though as with so many electronic structure descriptions, it is almost exclusively subjective.
[40] R. Kirmse, J. Stach, W. Dietzsch, E. Hoyer, Inorg. Chim. Acta 26 (1978) L53.
[41] J. Stach, R. Kirmse, W. Dietzsch, R.-M. Olk, E. Hoyer, Inorg. Chem. 23 (1984) 4779.
[42] D.T. Sawyer, G.S. Srivatsa, M.E. Bodini, W.P. Schaefer, R.M. Wing, J. Am. Chem. Soc. 108 (1986) 936.
[43] C.L. Beswick, J.M. Schulman, E.I. Stiefel, Prog. Inorg. Chem. 52 (2004) 55.
[44] K. Ray, T. Weyhermüller, A. Goossens, M.W. Crajé, K. Wieghardt, Inorg. Chem. 42 (2003) 4082.
[45] S. Kokatam, K. Ray, J. Pap, E. Bill, W.E. Geiger, R.J. LeSuer, P.H. Rieger, T. Weyhermüller, F. Neese, K. Wieghardt, Inorg. Chem. 46 (2007) 1100.
[46] G.N. Schrauzer, V.P. Mayweg, H.W. Finck, U. Müller-Westerhoff, W. Heinrich, Angew. Chem. 76 (1964) 345.
[47] G.N. Schrauzer, H.W. Finck, V.P. Mayweg, Angew. Chem. 76 (1964) 715.
[48] (a) R. Eisenberg, J.A. Ibers, J. Am. Chem. Soc. 87 (1965) 3776;
(b) R. Eisenberg, J.A. Ibers, Inorg. Chem. 5 (1966) 411;
(c) R. Eisenberg, W.W. Brennessel, Acta Cryst C62 (2006) m464.
[49] A.E. Smith, G.N. Schrauzer, V.P. Mayweg, W. Heinrich, J. Am. Chem. Soc. 87 (1965) 5798.
[50] R. Eisenberg, E.I. Stiefel, R.C. Rosenberg, H.B. Gray, J. Am. Chem. Soc. 88 (1966) 2874.
[51] R. Eisenberg, H.B. Gray, Inorg. Chem. 6 (1967) 1844.
[52] R. Eisenberg, Prog. Inorg. Chem. 12 (1970) 295.
[53] E.I. Stiefel, L.E. Bennett, Z. Dori, T.H. Crawford, C. Simo, H.B. Gray, Inorg. Chem. 9 (1970) 281.
[54] Dithiolene Chemistry: Synthesis, Properties, and Applications, Prog. Inorg. Chem. 52 (2004).
[55] The magnitude of the twist angle Θ is a function of the bite angle of a bidentate ligand. The normalized bite angle is defined as the distance between the donor atoms of the chelate divided by the metal-ligand bond length (D.L. Kepert, Prog. Inorg. Chem. 23 (1977) 1). From this value, an octahedral limit (Θlim) can be determined for any given complex. Here, Θlim for aromatic dithiolates are typically smaller than for more flexible olefinic dithiolenes.
[56] M.L. Kirk, R.L. McNaughton, M.E. Helton, Prog. Inorg. Chem. 52 (2004) 194.
[57] C. Milsmann, S. Sproules, E. Bill, T. Weyhermüller, S. DeBeer George, K. Wieghardt, Chem. Eur. J. 16 (2010) 3628.
[58] P. Banerjee, S. Sproules, T. Weyhermüller, S. DeBeer George, K. Wieghardt, Inorg. Chem. 48 (2009) 5829.
[59] R.R. Kapre, E. Bothe, T. Weyhermüller, S. DeBeer George, N. Muresan, K. Wieghardt, Inorg. Chem. 46 (2007) 7827.
[60] A. Davison, N. Edelstein, R.H. Holm, A.H. Maki, Inorg. Chem. 4 (1965) 55.
[61] J.A. McCleverty, J. Locke, E.J. Wharton, M. Gerloch, J. Chem. Soc. A (1968) 816.
[62] J.A. McCleverty, E.J. Wharton, J. Chem. Soc. A (1969) 2258.
[63] W.-L. Kwik, E.I. Stiefel, Inorg. Chem. 12 (1973) 2337.
[64] A. Davison, N. Edelstein, R.H. Holm, A.H. Maki, J. Am. Chem. Soc. 86 (1964) 2799.
[65] (a) S. Herzog, Z. Anorgm, Z. Anorg. Allg. Chem. 294 (1958) 155;
(b) R.N. Rogers, G.E. Pake, J. Chem. Phys. 33 (1960) 1107.
[66] S. Sproules, T. Weyhermüller, S. DeBeer, K. Wieghardt, Inorg. Chem. 49 (2010) 5241.
[67] (a) S. Bhattacharya, B.K. Kanungo, S. Sahoo, J. Coord. Chem. 59 (2006) 371;
(b) L.F. Larkworthy, M.W. O'Donoghue, Inorg. Chim. Acta 74 (1983) 155;
(c) T.L. Reichel, L.J. DeHayes, D.T. Sawyer, Inorg. Chem. 15 (1976) 1900.
[68] (a) W.E. Broderick, E.M. McGhee, M.R. Godfrey, B.M. Hoffman, J.A. Ibers, Inorg. Chem. 28 (1989) 2902;
(b) G. Chung, R. Bereman, P. Singh, J. Coord. Chem. 33 (1994) 331;
(c) C. Livage, M. Fourmigué, P. Batail, E. Canadell, C. Coulon, Bull. Soc. Chim. Fr. 130 (1993) 761;
(d) J.H. Welch, R.D. Bereman, P. Singh, Inorg. Chem. 27 (1988) 2862.
[69] G.N. Schrauzer, V.P. Mayweg, J. Am. Chem. Soc. 88 (1966) 3235.
[70] E.J. Wharton, J.A. McCleverty, J. Chem. Soc. A (1969) 2258.
[71] H.H. Downs, R.M. Buchanan, C.G. Pierpont, Inorg. Chem. 18 (1979) 1736.
[72] (a) Y. Sato, N. Tanaka, Bull. Chem. Soc. Jpn. 42 (1969) 1021;
(b) M.C. Hughes, J.M. Rao, D.J. Macero, Inorg. Chim. Acta 35 (1979) L321;
(c) T. Saji, S. Aoyagui, J. Electroanal. Chem. 63 (1975) 405.
[73] (a) S.S. Isied, G. Kuo, K.N. Raymond, J. Am. Chem. Soc. 98 (1976) 1763;
(b) K.N. Raymond, S.S. Isied, L.D. Brown, F.R. Fronczek, J.H. Nibert, J. Am. Chem. Soc. 98 (1976) 1767;
(c) S.R. Sofen, D.C. Ware, S.R. Cooper, K.N. Raymond, Inorg. Chem. 18 (1979) 234.
[74] (a) R.M. Buchanan, J. Clafin, C.G. Pierpont, Inorg. Chem. 22 (1983) 2552;
(b) C.G. Pierpont, Inorg. Chem. 40 (2001) 5727;
(c) C.G. Pierpont, H.H. Downs, J. Am. Chem. Soc. 98 (1976) 4834.
[75] (a) H.-C. Chang, S. Kitagawa, Angew. Chem. Int. Ed. 41 (2002) 130;
(b) H.-C. Chang, H. Myasaka, S. Kitagawa, Inorg. Chem. 40 (2001) 146.
[76] D.J. Gordon, R.F. Fenske, Inorg. Chem. 21 (1982) 2907.
[77] C. Milsmann, A. Levina, H.H. Harris, G.J. Foran, P. Turner, P.A. Lay, Inorg. Chem. 45 (2006) 4743.
[78] R.R. Kapre, E. Bothe, T. Weyhermüller, S. DeBeer George, K. Wieghardt, Inorg. Chem. 46 (2007) 5642.
[79] (a) G.R. Lewis, I. Dance, J. Chem. Soc. Dalton Trans. (2000) 3176;
(b) A. Sequeira, I. Bernal, J. Cryst. Mol. Struct. 3 (1973) 157.
[80] (a) T. Birchall, N.N. Greenwood, J. Chem. Soc. A (1969) 286;
(b) T. Birchall, N.N. Greenwood, J.A. McCleverty, Nature 215 (1967) 625.
[81] C.-H. Lin, C.-G. Chen, M.-L. Tsai, G.-H. Lee, W.-F. Liaw, Inorg. Chem. 47 (2008) 11435.
[82] A.L. Tenderholt, R.K. Szilagyi, R.H. Holm, K.O. Hodgson, B. Hedman, E.I. Solomon, Inorg. Chem. 47 (2008) 6382.
[83] D. Fomitchev, B.S. Lim, R.H. Holm, Inorg. Chem. 40 (2001) 645.
[84] B.S. Lim, J. Donahue, R.H. Holm, Inorg. Chem. 39 (2000) 263.
[85] S. Campbell, S. Harris, Inorg. Chem. 35 (1996) 3285.
[86] S. Sproules, S. DeBeer, K. Wieghardt, unpublished results.

[87] S. Sproules, F.L. Benedito, E. Bill, T. Weyhermüller, S. DeBeer George, K. Wieghardt, Inorg. Chem. 48 (2009) 10926.
[88] E.I. Stiefel, R. Eisenberg, R.C. Rosenberg, H.B. Gray, J. Am. Chem. Soc. 88 (1966) 2956.
[89] Harry had a penchant from adding elaborate footnotes to his early publications on dithiolene chemistry, so in that spirit, we note that the original paper on the electronic structure of $[Re(L_3)]^0$, where the predicted ground state of $(4e')^2(2a_2')^2(3a_1')^1(5e')^0$ was amplified to address the question of oxidation states. The authors considered two extremes: (1) that the $4e'$ orbitals were derived from Re $5d_{x^2-y^2,xy}$ orbitals while the empty $5e'$ MOs as essential ligand-based. This gave a d^5 electron count (four electrons in the $4e'$; one electron in the $3a_1'$) and the complex was formulated as $[Re^{II}(L_3^{2-})]^0$ with the ligand unit having, in our more modern parlance, four valence holes – the vacant $5e'$ level; and (2) that the $4e'$ orbitals were predominantly ligand in character and the Re $5d_{x^2-y^2,xy}$ orbitals constituted the empty $5e'$ MOs. This led to an $[Re^{VI}(L_3^{6-})]^0$ description with the unpaired electron in the Re $5d_{z^2}$ orbital and the tris(dithiolene) unit fully reduced. The calculation performed at the time gave no bias to either description, in that it was reported that the $4e'$ MOs were equally divided between the metal and ligands, such that the true electronic structure lay somewhere between $[Re^{II}(L_3^{2-})]^0$ and $[Re^{VI}(L_3^{6-})]^0$. Having been asked on more than one occasion about the composition of these filled $4e'$ orbitals that could potentially undermine our Re(V) oxidation state assignment, we note that based on the ZORA/B3LYP DFT calculations performed on the $[Re(bdt)_3]^{1+/0/1-}$ series, the Re 5d contribution to the Löwdin reduced orbital population for each $4e'$ orbital is consistently <10% across the series irrespective of the trigonal twist angle (geometry optimized at 0° for the monocation to 24.9° for the monoanion). Therefore, the traditional assignment of the $4e'$ orbitals as ligand-based is entirely valid. Furthermore, the calculated 3d contribution to the $4e'$ MOs in the $[V^{IV}(pdt)_3]^{0/1-/2-}$ series are (per orbital) 12.8%, 11.9%, and 15.4%, respectively. Even though the V 3d manifold lies energetically closer to the ligand orbitals compared to the Re 5d manifold, there is only a minor increase to the metal contribution of the $4e'$ level.
[90] A.H. Al-Mowali, A.L. Porte, J. Chem. Soc. Dalton Trans. (1975) 250.
[91] S. Sproules, T. Weyhermüller, K. Wieghardt, unpublished results.
[92] (a) J. Locke, J.A. McCleverty, E.J. Wharton, C.J. Winscom, Chem. Commun. (1966) 677;
(b) J.A. McCleverty, N.M. Atherton, J. Locke, E.J. Wharton, C.J. Winscom, J. Am. Chem. Soc. 89 (1967) 6082.
[93] (a) A.L. Balch, I.G. Dance, R.H. Holm, J. Am. Chem. Soc. 90 (1968) 1139;
(b) J.A. McCleverty, Prog. Inorg. Chem. 10 (1968) 49.